# Identification of atmospheric and oceanic teleconnection patterns in a 20-year global data set of the atmospheric water vapor column measured from satellites in the visible spectral range

Thomas Wagner[1] and Steffen Beirle[1], Steffen Dörner[1], Christian Borger[1], Roeland Van Malderen[2]

[1]Satellite Remote Sensing Group, Max Planck Institute for Chemistry, Mainz, Germany
[2]KMI – IRM, Royal Meteorological Institute of Belgium, Brussels, Belgium

*Correspondence to*: Thomas Wagner (thomas.wagner@mpic.de)

**Abstract.** We used a global long-term (1995-2015) data set of total column water vapor (TCVW) derived from satellite observations to quantify to which extent the temporal patterns of various teleconnections can be identified in this data set. To our knowledge, such a comprehensive global TCWV data set was rarely used for teleconnection studies. One important property of the TCWV data set is that it is purely based on observational data. We developed a new empirical method to decide whether a teleconnection index is significantly detected in the global data set. Based on this method more than 40 teleconnection indices were significantly detected in the global TCWV data set derived from satellite observations. In addition to the satellite data we also applied our method to other global data sets derived from ERA-Interim. One important finding is that the spatial patterns obtained for the ERA TCWV data are very similar to the observational TCWV data set indicating a high consistency between the satellite and ERA data. Moreover, similar results are also found for two selections of ERA data (either all data or mainly clear sky data). This finding indicates that the clear-sky bias of the satellite data set is negligible for the results of this study. However, for some indices, also systematic differences in the spatial patterns between the satellite and model data set were found probably indicating possible shortcomings in the model data. For most 'traditional' teleconnection data sets (surface temperature, surface pressure, geopotential heights and meridional winds at different altitudes) a smaller number of significant teleconnection indices was found than for the TCWV data sets, while for zonal winds at different altitudes, the number of significant teleconnection indices (up to >50) was higher. The strongest teleconnection signals were found in the data sets of tropospheric geopotential heights and surface pressure. In all global data sets, no 'other indices' (solar variability, stratospheric AOD or hurricane frequency) were significantly detected. Since many teleconnection indices are strongly correlated, we also applied our method to a set of orthogonalised indices, which represent the dominant independent temporal teleconnection patterns. The number of significantly detected orthogonalised indices (20) was found to be much smaller than for the original indices (42). Based on the orthogonalised indices we derived the global spatial distribution of the cumulative effect of teleconnections. The strongest effect on the TCWV is found in the tropics and high latitudes.

## 1 Introduction

It has been known for a long time that weather at one location can be linked to weather at a far distant location (Walker and Bliss, 1932; Bjerknes, 1966, 1969; Wallace and Gutzler, 1981; Nigam and Baxter, 2015; Feldstein and Frantzke, 2017 and references therein). The distances between such locations can be very large, up to opposite locations on the globe. The strength of the correlation varies with location exhibiting regions of maximum (anti-) correlations and regions without any significant correlation. The resulting correlation patterns are referred to as teleconnection patterns. The strongest teleconnection is the El-Nino / Southern oscillation (ENSO) phenomenon (Walker and Bliss, 1932; Bjerknes, 1966, 1969), but many more teleconnection are known, which are located in many regions on both hemispheres (e.g. Feldstein and Frantzke, 2017 and references therein).

The temporal variability of teleconnections is usually described by teleconnection indices (e.g. the ratio of surface pressures at selected stations) and covers a wide range of frequencies from a few days to inter-annual and inter-decadal time scales (Hurrel, 1995; Feldstein, 2000; Nigam and Baxter, 2015; Woolings et al., 2015; Feldstein et al., 2017). Atmospheric teleconnections (like e.g. the North Atlantic Oscillation, NAO) have typically higher intrinsic frequencies than oceanic teleconnection indices (like e.g. the Atlantic Meridional Mode, AMM).

Teleconnections can be identified in different data sets like sea level pressure, surface air temperature, sea level pressure as well as geopotential heights and wind fields at different altitudes (Wallace and Gutzler, 1981; Thompson and Wallace, 1998; Nigam and Baxter, 2015; Feldstein and Frantzke, 2017). In recent studies, the geopotential height is the most used variable for the quantification of teleconnections. Teleconnections are mainly found in the troposphere with the strongest amplitudes in the upper troposphere (Feldstein, 2000). But several teleconnections have also connections to the stratosphere (Feldstein, 2000 and references therein; Nigam and Baxter, 2015; Feldstein and Frantzke, 2017; Domeisen et al., 2019). Teleconnections can be identified and defined in different ways: historically, teleconnection indices were empirically and intuitively determined based on the locations of meteorological stations (e.g. Walker and Bliss, 1932). In later studies more objective methods were developed based on correlation matrices, principle component analyses (PCA) (also referred to as empirical orthogonal function (EOF) methods) or rotated PCA (also referred to as varimax rotation). More details about these and further methods can be found in Horel (1981), Wallace and Gutzler (1981), Barnston and Livezey (1987), Thompson and Wallace (1998), Feldstein and Frantzke (2017) and references therein. If these methods are applied, the derived teleconnections time series and spatial patterns particularly depend on the selected region of the globe. Most of such studies use pressure or geopotential heights and are confined to midlatitude and Arctic regions in the Northern Hemisphere because of the barotropic conditions in the tropical latitudes. Thus usually, these methods are not applied for the full globe.

Besides the fact that teleconnections are interesting in themselves, their study is also important for other applications. For example, taking teleconnections into account can improve weather forecasts (Feldstein and Frantzke, 2017 and references therein). They have impact on extreme events, e.g. heat waves, droughts, and floods (King et al., 2016; Yeh et al., 2018 and references therein) and can affect storm tracks. In addition to atmospheric quantities (e.g. humidity, precipitation, stratospheric ozone), teleconnections also affect oceanic variables (e.g. Arctic and Antarctic sea ice, the Atlantic thermohaline circulation) and the marine and terrestrial ecosystems (Feldstein and Frantzke, 2017 and references therein). Finally it is worth noting that teleconnections are expected to change in a changing climate (e.g. King et al., 2016; Feldstein and Frantzke, 2017; Yeh et al., 2018).

In this study we investigate to which extent the temporal patterns of various teleconnections can be identified in the global distribution of the total column water vapor (TCWV). For that purpose we use a consistent long term data set (1995 – 2015) derived from satellite observations in the visible spectral range obtained from GOME on ERS-2, SCIAMACHY on ENVISAT and GOME-2 on MeTop (Beirle et al., 2018). The data sets consist of monthly mean values on a 1° x 1° latitude/longitude grid, which were carefully merged making use of the long overlap time between the different satellite data sets (for details see Beirle et al., 2018). Validation by independent data sets showed a smooth temporal variation with a stability within 1% over the whole period (1995-2016) (Danielczok and Schröder, 2017). To our knowledge, teleconnection studies using water vapor data sets are rare (e.g. van Malderen et al., 2018). One particular specialty / advantage of our study is that we use for the first time a global data set which is entirely based on measurements. Here it is important to note that the TCWV is dominated by the atmospheric layers close to the surface. Another important aspect of our study is the development of a new empirical method to decide whether a teleconnection (index) can be significantly identified in an atmospheric data set or not.

Our study addresses the following main questions:

a) Which teleconnection index (and other time series such as indices of solar activity) can be significantly identified in the satellite TCWV data set (or other data sets)? Here it should be noted that we do not aim to identify causal relationships or even to predict the TCWV based on teleconnection indices.

b) Are the same results obtained for TCWV data from observations and models? Here also the question is addressed how representative the satellite observations (for mainly clear sky) are for all sky data sets. Another important aspect is to compare the spatial patterns obtained for the different teleconnections between the satellite and model data sets. Such differences can give hints on possible shortcomings of the model simulations or measurements.

c) How does the number of significant teleconnections in the global TCWV data sets compare to similar results obtained for "traditional" teleconnection data sets like surface temperature, sea level pressure or wind fields and geopotential heights at different altitudes? From this comparison we can conclude whether our global TCWV data set is suited for teleconnection studies. One advantage of the use of this TCWV data set is that it is exclusively derived from measurements.

d) What is the spatial distribution of teleconnection patterns found in the global TCWV distribution? One motivation for this question is that the different teleconnections have specific drivers (e.g. tropical convection). Thus the obtained spatial distributions can give hints on the underlying mechanisms.

The paper is organised as follows: In section 2 the global data sets used in this study, and in section 3 the considered (mostly teleconnection) indices are introduced. Section 4 presents the fit function of the indices to the global data sets and the obtained global patterns. In section 5 a new method for the determination of the significance is introduced, which is applied to the different global data sets in section 6. In section 7 a reduced set of orthogonalised teleconnection indices is extracted and. Section 8 presents the global distribution of the cumulative effect of the teleconnections.

**2 Data sets**

**2.1 Total water vapor column**

Our study focuses on global long term data sets of the total column water vapor (TCWV). Here we use three data sets:

a) Satellite observations from July 1995 to October 2015 (Beirle et al., 2018) derived from the satellite instruments GOME on ERS-2 (1995 to 2003), SCIAMACHY on ENVISAT (2002 to 2012) and GOME-2 on MetOp (2006 to present), which have similar overpass times (between 9:30 and 10:30 LT). The data analysis is performed in the red spectral range. Since these satellite instruments observe scattered and reflected sun light, the observations are sensitive for the whole atmospheric column including the surface-near layers which usually contain the largest fraction of the total atmospheric TCWV. The start date of the time series was predetermined by the start of the first satellite mission; the end date of the time series was set to October 2015, because some of the used time series were only available until that date. The data set is available on a 1° x 1° latitude/longitude grid with monthly resolution. The data set does not cover polar winter, since the satellite observations use scattered and reflected sun light.

In Fig. 1 the variation of the TCWV with latitude and time is shown (the latitude bins represent zonally averaged values). The top panel shows the original TCWV data set, whereas both lower panels present the absolute and relative anomalies with the mean seasonal cycle removed. Several anomaly patterns are clearly obvious, which are mainly related to strong ENSO events (see e.g. Soden, 2000; Simpson et al., 2001; Wagner et al., 2005). Especially for the relative anomalies, many high frequency variations are found. While part of these high frequency variations represent measurement noise and atmospheric noise, the results of this study showed that they also represent atmospheric teleconnections.

In addition to the satellite observations of the TCWV we also use global time series of the TCWV derived from ECMWF reanalysis (ERA Interim, Dee et al., 2011). Here we use two data sets:

a) All ERA data including clear and cloudy conditions

b) Only ERA data for clear sky observations. Here, a cloud cover below 0.3 between 1km and 6km is regarded as cloud free. This criterion reflects the observational conditions of the satellite data set.

Both data sets have a temporal resolution of 6h. For the comparison with the satellite TCWV results, the ERA data were temporally interpolated to the time of the satellite overpass (10:00 LT). From the comparison of the results for the measurements and model data sets, the effect of the specific sampling of the satellite observations (which represent only clear sky observations) can be investigated. In Fig. 2 the global mean distributions of the TCWV data sets from satellite observations and ERA data are shown. Similar patterns are found in all three data sets indicating the good consistency amongst them. The highest values are found over the tropics, especially over the west Pacific. Lower values are found towards higher latitudes showing the strong dependence of the TCWV on temperature.

## 2.2 Other global data sets

Teleconnections patterns are usually derived from meteorological quantities like surface pressure and temperature or geopotential heights and wind fields at different altitudes. In this study we also consider such quantities, which we also obtained from ERA data (see Table 1). We analyse these data sets similarly to the TCWV data sets (details are described below). In this way we will assess in how far the impact of teleconnections on TCWV is comparable to traditional teleconnection data sets.

## 3 Teleconnection indices

We performed an extensive search for teleconnection indices in the scientific literature and web sites of national weather services. We found in total 54 teleconnection indices, which cover the time span of our TCWV data set. An overview on these teleconnection indices as well as additional time series (e.g. of the solar activity) is given in Table 2. Although we do not only focus on teleconnection indices in this study, in the following we use the term 'index' to describe the whole set of teleconnection indices and other time series.

It should be noted that for several teleconnection indices (in particular for the Madden-Julian oscillation) different definitions exist. Thus the number of teleconnection indices in Table 2 is much larger than the corresponding atmospheric phenomena. Many of these indices (describing the same phenomenon), but also many of the other teleconnection indices are highly correlated. The strength of these correlations is presented in Fig. 3 as a matrix with correlation coefficients between the different indices (after the seasonal cycles were removed). In spite of the correlations amongst the teleconnection indices, we decided as a first step to include them all in our study, because beforehand it is not clear which index might be best suited to represent a teleconnection phenomenon. Using our empirical approach, however, it becomes possible to quantify the significance and strength of the different indices and thus to select the best suited index for a given teleconnection phenomenon. Finally, we apply an orthogonalisation for the most significant indices (see section 7) to minimise the effect of the correlations and to identify the dominant temporal teleconnection patterns in our TCWV data set.

A detailed overview on the selected indices and their data sources is provided in Fig. A6 in the appendix.

## 4 Analysis of global data sets

To determine the strength with which individual indices are detected in the temporal variations of the different global data sets, the index time series are fitted to the global data sets as described in section 4.1 below. Before the fit is applied, the mean seasonal cycle (1995 – 2015) and a linear trend are subtracted from the individual indices (see e.g. Horel 1981). Some

170 teleconnection indices are characterised by strong seasonal cycles, whereas others are not. Finally the obtained anomalies are normalised by the corresponding standard deviations. This ensures that the obtained fit coefficients for the different indices can be directly compared. The different steps of these preparations are illustrated in Fig. A7. For consistency, the same steps are also applied to the different global data sets before the fit is applied.

175 **4.1 Fit function**

For each 1° x 1° latitude / longitude pixel of the global data sets (the example below is for the TCWV) the de-seasonalised time series of the monthly mean anomalies are fitted by the following function:

180 $$TCWV_i(t) = c + b \cdot t + f_i \cdot index_i(t)$$ (1)

Here c and b describe constant and linear terms. $index_i$ represents the selected normalised index of monthly mean anomalies. The fit coefficient $f_i$ describes the sign and strength of the contribution of the chosen index to the variability of the TCWV anomaly of the chosen 1° x 1° pixel. The constant offset b and possible linear trend c and the fit coefficient $f_i$ are 185 simultaneously determined by the fit. An example of the derived fit coefficient for the ENSO index is shown in Fig. 4 (top). Systematic patterns with positive and negative fit coefficients are found. The fit function is separately applied to the individual indices listed in Table 2. Here it should be noted that the fit function could in principle be applied to several or even all indices simultaneously. However, since many indices are highly correlated, the interpretation of the results would then not be straight forward. Thus, we chose to include the individual indices one by one in the fit function. Besides the 190 parameters c, b, and the fit coefficient $f_i$, also the difference between the temporal variation of the global data sets and the applied fit function is quantified by the root mean square (RMS). The RMS for the ENSO index is shown in Fig. 4 (second row).

In order to quantify the importance of a selected index, a second fit is performed with only the constant and linear terms:

195 $$TCWV(t) = c + b \cdot t$$ (2)

The comparison of the RMS with and without including the index term (eqs. 1 and 2) allows to quantify the importance of the chosen index to describe the temporal variation of the data set. Therefore the following quantity is defined:

200 $$delta\ RMS = \frac{RMS_{without\ index} - RMS_{with\ index}}{mean\ of\ data\ set(latitude)}$$ (3)

The RMS differences are divided by the zonal mean value (see appendix 1) of the considered quantity, because (like for water vapor) many of the analysed quantities depend strongly on latitude. The delta RMS is a measure for the magnitude of the variance of a considered data set, which can be explained by the chosen teleconnection pattern. If there is high similarity 205 of the temporal variation of an index with the temporal variation of the considered data set, the delta RMS values for both fits is large. If there is no similarity, the corresponding delta RMS value is zero.

It should be noted that instead of the delta RMS values, also the correlation coefficients between the considered data set and 210 the fit function (eq. 1) might have been used since the spatial patterns of both quantities are very similar (see Fig. A8).

The delta RMS value for the ENSO index is also shown in Fig. 4 (bottom).

The fit results in Fig. 4 for the ENSO index are obtained for the TCWV from satellite observations (left), ERA data (center), and ERA data for clear sky conditions (right). High fit coefficients (Fig. 4 top) mean that a substantial part of the measured

TCWV time series can be explained by the ENSO index pattern. High negative fit coefficients mean the same for the negative ENSO index. Fit coefficients of zero indicate no connection to ENSO. Very similar spatial patterns are found for the three TCWV data sets indicating that the ENSO phenomenon is well captured in the satellite and model data sets. From the similarity between the model data including all sky conditions (center) or only clear sky conditions (right) it can be concluded that the satellite observations (representing mainly clear sky conditions) are representative for all sky conditions (no obvious clear sky bias).

In all three data sets, the smallest RMS (Fig. 4, second row) are found close to the equator. This is an interesting finding, but can probably be explained by a) the rather high TCWV and b) its rather small variability in these regions. In mid-latitudes, systematically higher RMS are found for the satellite observations compared to the model results. This is probably related to the rather large effects of clouds on the satellite observations, which becomes especially important in these regions (clouds lead to less valid observations and larger measurement uncertainties). Another interesting finding is that in polar regions the RMS for the satellite observations is smaller than for the model results. This finding is probably related to the sparseness of water vapor measurements in these regions assimilated in the ECMWF model. Thus the spatio-temporal variability of the satellite observations is probably more realistic than that of the model data. The RMS for the model results for clear sky conditions is slightly higher than for the model results for all conditions, which is to be expected because of the reduced number of data available for the cloud-filtered data set.

The lower panel of Fig. 4 shows the delta RMS for the ENSO index indicating the reduction of the RMS if the ENSO index is included in the fit. As expected, the largest delta RMS is found over the tropical Pacific, where the ENSO phenomenon is most pronounced. The global distribution of the delta RMS is very similar for the three data sets. The fit coefficients and delta RMS for three other selected indices are shown in Fig. 5 for the TCWV data set from satellite observations. For all indices, specific activity centers can be found in different parts of the globe. The fit coefficients for all indices are presented in the appendix (Fig. A9). Note that in general very similar spatial patterns are found for the three TCWV data sets, but in some cases also systematic differences are derived (for more details see section 6.1). As expected, for groups of indices with strong temporal correlation also similar spatial patterns are found. This is most obvious for indices similar to the ENSO index (first group of indices in Figures A6 and A8). Similar spatial patterns are also found for other pairs of indices, e.g. between the Hawaiian Index (HAW) and the Pacific Decadal Oscillation (PDO) as well as between the South Tropical Atlantic index (STA) and the Equatorial Atlantic Index (EA_errst).

## 5 Determination of significance

For most teleconnection indices spatially coherent patterns of fit coefficients and delta RMS values are found in the global maps (see Fig. A9) indicating that these indices are significantly detected in the global water vapor data sets. These spatial patterns agree also well to the known regions where the corresponding teleconnections are active. Information about the significance of the fit results can be obtained from the fit function itself. However, in practice, the significance information from the fit has several limitations:

a) The determination of the significance is based on several assumptions about the data sets, e.g. that all data points of the time series have the same uncertainties and follow a normal distribution. However, the errors of the individual data points can be very different, e.g. the effect of clouds on the errors of the satellite TCWV data set can be very different for different seasons and regions. Also, the uncertainties are not only random but contain also systematic contributions. It is difficult (if not impossible) to quantify the uncertainties of the involved time series.

b) The determination of the significance is based on prescribed significance levels. The choice of such a significance level is arbitrary and the obtained significance information depends on this choice.

c) In several tests we fitted artificial time series to the TCWV data set. These tests showed that even for such non-geophysical time series 'significant' fit results can be obtained (see the examples in Fig. 6). On the left side of this figure, fit results for a time series containing only white noise, and on the right side fit results for a temporally reversed teleconnection index are shown (the temporally reversed index is obtained from the original index by mirroring the time axis). The blue and red areas show fit coefficients for both time series, which are classified as significant by the fit.

Based on these findings, we conclude the use of the significance of the detection of an index derived from the fit itself is not straight-forward.

To address these difficulties, we developed and applied an empirical approach to determine threshold values for the delta RMS values to decide whether an index is significantly detected in a global data set. The new procedure is described in the next section. It has the following two main advantages:

-the threshold values are determined empirically. Thus no assumptions on the properties of the time series or the significance levels have to be made.

- the method provides a clear procedure and in particular a metric which can be applied in a consistent way to different data sets and thus allows a quantitative comparison (see section 6).

## 5.1 Use of reversed indices

The basic idea of our new approach is to use non-geophysical indices for the estimation of the significance level. Non-geophysical indices are indices without any temporal correlation with the temporal variations of the investigated geophysical data sets. For that purpose we chose all temporally reversed indices (see Table 2 and Fig. A6), because they cover all relevant frequencies of the true teleconnections. In practice, the time axis is flipped, that means the first entry (July 1995) will be assigned to the last month (October 2015), and so on. In a first step, we calculate the 99th percentile of the delta RMS values of the reversed indices for all 1° x 1° pixels of the global map. We chose the 99th percentile because it is close to the maximum, but still not affected by individual outliers. The red data points in Fig. 7 presents the 99th percentiles (p99) for all reversed indices for the three TCWV data sets. From the mean value and standard deviation of the results for all temporally reversed indices, we calculate a threshold value (black dotted line in Fig. 7) for each data set (for details see appendix A2). The obtained threshold value for the TCWV data set from satellite observations is 0.0031. We also applied the same method to a set of artificial random time series and obtained a very similar threshold value of 0.0033 confirming that the threshold value obtained from the temporally reversed time series is reasonable.

If the p99 values are above the threshold, it is likely that the considered index significantly contributes to the variability of the considered data set and vice versa.

In Fig. 7 besides the p99 values for the temporally reversed indices (red), also those for the original indices are shown (blue). For many of the original indices, the p99 values are much larger than the threshold value indicating that these indices are significantly detected in the respective data set.

In addition to the use of the absolute threshold of the delta RMS values for the determination of significance, we also made use of the effect of time shifts applied to the individual indices. The underlying idea is that the delta RMS values should decrease if the original indices are de-synchronised by ± 1 month. The details of this approach are described in appendix A3. Using this additional criterion, a few more indices are added to the number of significantly detected teleconnection indices. For the TCWV data set from satellite observations, the number of significantly detected indices increases from 40 to 42, for the ERA TCWV data set from 43 to 44, and for the ERA data set for clear sky conditions from 39 to 42.

## 6 Comparison of the results for the different global data sets

A rather high number of significant indices was identified in the global TCWV data sets. To put this finding into a broader perspective, we applied the same procedure also to other global data sets, which are usually considered in teleconnection studies (see Table 1). The corresponding p99 values of the different indices (including also the reversed indices) are presented in Fig. A10. In general similar results as for the TCWV data sets are found. In particular, for all data sets a large number of teleconnection indices is significantly detected. However, also differences are found: in particular, the teleconnection index with the maximum p99 value is found to be different for the different data sets. For the TCWV data sets, surface temperature and pressure, as well as most of the zonal winds, the largest p99 values are found for indices similar to ENSO. For the TCWV data sets and surface temperature, this can be expected, because the ENSO phenomenon is driven by the surface temperature (over the tropical Pacific). Accordingly, also the TCWV data sets will be strongly affected, because the TCWV depends strongly on the temperature in the lowest atmospheric layers. The strong influence of the ENSO phenomenon (BEST index) on the zonal winds at most levels can probably be explained by the fact that large scale phenomena like ENSO can have a strong influence on the quasi-persistent zonal flow patterns in the tropics and sub-tropics. For the geopotential heights and meridional winds, the largest p99 values are found for the polar atmospheric indices (mostly AAO, but also SCA). For the geopotential heights this might be expected because the polar atmospheric indices are defined based on anomalies of the geopotential heights. Why also for the zonal winds, the largest p99 values are found for the polar atmospheric indices is, however, is not clear to us.

A summary of the number of significant indices and the teleconnection index with the highest p99 is given in Table 3. Most significant indices are found for the zonal winds with the highest number in the upper troposphere. For these data sets the number of significant indices is larger than for the TCWV data sets. For geopotential heights and meridional winds, less significant indices are found (and even less than for the TCWV data sets). For geopotential heights most significant indices are found in the upper troposphere, while for the meridional winds no clear altitude dependence is observed. Also for the surface temperature and surface pressure rather low numbers (less than for the TCWV data sets) of significant indices are found. From these results we conclude that the global TCWV data sets are well suited for teleconnection studies. Here it should again be noted that the satellite TCWV data is exclusively determined from measuremensts, and the TCWV is dominated by the layers close to the surface. Thus our findings indicate that also indices which are usually detected in the middle and upper troposphere can be significantly detected in data sets which are dominated by the lower troposphere.

Our new method for the determination of the significance level also allows a direct comparison of the strengths at which the different indices are detected in the different data sets. In Table 3 also the maximum p99 values of the delta RMS normalised by the corresponding significance threshold values are shown. The highest normalised p99 values are found for the geopotential heights (except the 50hPa level) and the surface pressure. This finding is consistent with the fact that these quantities are used in most teleconnection studies and many indices are even defined using these quantities. The lowest normalised p99 values are found for zonal winds, for which also the smallest numbers of significant indices are obtained. Intermediate values are found for the water vapor data sets.

**6.1 Comparison of the spatial patterns of the measured and simulated TCWV**

For most of the teleconnection indices, very similar spatial patterns are found in the TCWV data sets obtained from satellite or ECMWF data (see Fig. A9). This confirms both the high quality of the satellite measurements and model simulations. However, for some indices, also substantial differences are found (see Fig. 8). The most obvious differences are found over northern Africa. In principle, they could be caused by errors of both the satellite or model data sets. However, since very good agreement over northern Africa is found for most of the indices, we can very probably exclude systematic measurement biases (like e.g. effects from the high surface albedo over the Sahara). Thus we conclude that the observed

differences probably indicate deficiencies in the model simulations, possibly related to the sparseness of observational data over northern Africa used in the model. It is interesting to note that the differences are found for both oceanic and atmospheric indices which have rather different frequencies. These comparison results might help to improve the model performance over norther Africa (and to a lesser degree also over other regions).

## 7 Orthogonalisation of indices

It was shown in Fig. 3 that many indices are strongly correlated. Thus the numbers of ‚significant indices' obtained in the previous chapters are not useful to represent the number of independent significant indices. To account for correlations between the different indices, we thus applied an orthogonalisation approach. For the orthogonalisation (based on the Gram–Schmidt process), all ‚significant' original indices and significant temporal derivatives (see Figure A11) were considered (in total 57 indices). The order of indices used in the iterative orthogonalisation process was from highest to lowest p99 values. The result of the orthogonalisation approach is a set of modified teleconnection indices, which shows zero correlation amongst each other (for the considered time period). Thus this new set of orthogonalised indices can be used to determine the number of independent significant teleconnection patterns in the global water vapor data sets. We applied our new method to the new set of orthogonalised indices to test which of the modified indices have p99 values above the significance threshold. As expected, this number (20) was found to be much smaller than for the original indices (40) confirming that many teleconnection indices are indeed highly correlated and related to the same phenomena. We also found that the difference between the highest p99 value (for the ONI index) and subsequent p99 values is much larger than for the original indices. This finding indicates that the temporal pattern of the ENSO phenomenon is contained in many teleconnection indices (see also Fig. 3).

The delta RMS maps for the significant orthogonalised indices (together with the delta RMS maps for corresponding original indices) are presented in Fig. A12.

## 8 Global distributions

The delta RMS maps derived for the individual indices show characteristic patterns which indicate in which regions of the globe the selected index is important or not. In order to assess the global distribution of the general importance of teleconnections, we added the delta RMS maps of all significant indices. The corresponding maps of the derived cumulative delta RMS distributions are presented in Fig. 10 for different selections of teleconnection indices and TCWV data sets. In the upper panel the patterns of all significant teleconnection indices found for the TCWV data set from satellite observations are added. In the middle panel the same is shown for the significant orthogonalised indices. The comparison again clearly indicates that many indices are highly correlated to the ENSO index. Thus, if only the orthogonalised indices are considered, the ENSO pattern, especially in the tropical Pacific, becomes relatively weaker compared to the cumulative delta RMS values in other regions. The cumulative delta RMS map for the orthogonalised indices represents the overall contribution of teleconnections to the variability of the global TCWV distribution. Our results indicate that these contributions are strong in the Tropics as well as in high latitudes. This points to potential drivers of these teleconnections, e.g. tropical convection or synoptic-scale wave breaking in jet exit regions (see e.g. Feldstein and Franzke, 2017). In the lower panel the cumulative delta RMS map for all significant orthogonalised indices for the ERA TCWV data set is shown. The derived spatial patterns are very similar to those for the satellite data set. It should, however, be noted that also for regions in high latitudes, which are not covered by the satellite observations high values are found.

Fig. 11 shows the latitudinal (top) and longitudinal (bottom) distribution of the p99 values for all significant original indices (red) and all significant orthogonalised indices (blue) detected in the TCWV data from satellite observations. As expected,

the highest values (related to ENSO) are found over the equatorial east Pacific, but most indices have the strongest effects in mid and high latitudes. Interestingly, in the latitude range between −30° and +30° only for one significant orthogonalised index (besides ENSO) the maximum delta RMS is found.

**9 Conclusions**

We investigated if and how strong the temporal patterns of a large set of teleconnection indices can be identified in the spatio-temporal variability of a global data set of the total column water vapor (TCWV) from 1995 – 2015 derived from satellite observations. To our knowledge, it is the first time that a global TCWV data set was used in such a detailed way in teleconnection studies (note that part of this data set was already used by van Malderen et al., 2018). Here it is important to note that the TCWV data set is purely based on observational data. Another important achievement of this study is the development of a new empirical method to decide whether a teleconnection index is significantly detected in the global data set. The method is based on temporally reversed teleconnection indices, which ensures that all relevant time scales are considered. The new method can be applied in a universal way to different data sets. In this study we applied the new method to the TCWV sets derived from satellite or model data as well to several further quantities, which are often used in teleconnection studies. Based on the obtained results, we could derive the following main conclusions related to the science questions mentioned in the introduction:

a) We developed a new empirical approach to determine whether a teleconnection index is significantly detected in a global data set. This approach avoids problems of existing algorithms for the determination of significance, because no assumptions on the significance level or the measurement uncertainties have to be made. We applied the new method to a global data set of the TCWV derived from satellite observations and found that 40 teleconnection indices could be significantly detected.

b) We applied the same method also to TCWV from the ERA interim data set. Here we used two versions of the model data sets, one including all data, the other only clear sky data. The results for both versions agree in general very well with those for the satellite data set. This confirms both the quality of the satellite and model data sets. It also indicates that the satellite observations can be seen as representative for all day mean values. For some teleconnections, however, also systematic differences, mainly over northern Africa, were obtained. Since these differences are not found for the majority of the teleconnection indices, we conclude that they are very probably not related to systematic errors of the satellite data set, but rather indicate shortcomings of the model over these regions.

c) We also applied our method to a variety of other data sets, which are usually used in teleconnection studies (surface temperature, surface pressure, geopotential heights and meridional winds at different altitudes). For most of these data sets less teleconnection indices were significantly detected than for the TCWV data sets, while for zonal winds, more teleconnection indices (up to >50) were significantly detected. These results indicate that our global TCWV data set is well suited for teleconnection studies. In our view, this is an important aspect, because our data set is exclusively based on measurements. The strongest teleconnection signals were detected for the data sets of tropospheric geopotential heights and surface pressure. This finding is consistent to the fact that most teleconnection studies are based on these quantities. Another interesting finding is that in none of the global data sets, non-teleconnection indices (like the solar variability, the stratospheric AOD or the hurricane frequency) were significantly detected.

d) We investigated the spatial distribution of the teleconnection patterns. In particular we calculated global maps for the cumulative effect of all teleconnection patterns. For that purpose we first orthogonalised the teleconnection indices to avoid the effect of correlation between the indices. Compared to the original set of indices, much less of the orthogonalised indices (20 compared to 42) were significantly detected in the TCWV data set. Our global map of the cumulative effects of all significantly detected orthogonalsed teleconnections showed the strongest teleconnection signals in the global TCWV data

set over the Tropics and in polar regions. These spatial patterns point to importance of different driving mechanisms in different regions.

430

**Acknowledgements**

We want to thank the European Centre for Medium-Range Weather Forecasts (ECMWF) and many scientific and national

435 institutions for making meteorological data and teleconnection indices available. We also thank ESA and EUMETSAT for making satellite spectra available. We are grateful to Holger Sihler for his valuable feedback and suggestions about the discussion of the significance derived from the fit.

**Data availability**

440 The TCWV data from satellite observations are available through Beirle et al. (2018). Other data sets are available from the authors on request.

**Author contributions**

Thomas Wagner initiated this study. Thomas Wagner and Steffen Beirle performed the data analysis. Steffen Dörner

445 extracted the ECMWF data sets. Thomas Wagner, Steffen Beirle, Steffen Dörner, Christian Borger and Roeland Van Malderen contributed to the interpretation of the results of this study.

**Competing interests**

There are no competing interests.

450

**References**

Barnston, A.G., Livezey, R.E., Classification, seasonality and persistence of low frequency atmospheric circulation patterns. Monthly Weather Review 115, 1083–1126, 1987.

455 Beirle, S., Lampel, J., Wang, Y., Mies, K., Dörner, S., Grossi, M., Loyola, D., Dehn, A., Danielczok, A., Schröder, M., and Wagner, T.: The ESA GOME-Evolution "Climate" water vapor product: a homogenized time series of $H_2O$ columns from GOME, SCIAMACHY, and GOME-2, Earth Syst. Sci. Data, 10, 449-468, https://doi.org/10.5194/essd-10-449-2018, 2018.

Bjerknes, J., A possible response of the atmospheric Hadley circulation to equatorial anomalies of ocean temperature. Tellus, 18, 820–829, 1966.

460 Bjerknes, J., Atmospheric teleconnections from the equatorial Pacific. Monthly Weather Review, 97, 163–172, 1969.

Dee, D. P., S. M. Uppala A. J. Simmons P. Berrisford P. Poli S. Kobayashi U. Andrae M. A. Balmaseda G. Balsamo P. Bauer P. Bechtold A. C. M. Beljaars L. van de Berg J. Bidlot N. Bormann C. Delsol R. Dragani M. Fuentes A. J. Geer L. Haimberger S. B. Healy H. Hersbach E. V. Hólm L. Isaksen P. Kållberg M. Köhler M. Matricardi A. P. McNally B. M. Monge-Sanz J.-J. Morcrette B.-K. Park C. Peubey P. de Rosnay C. Tavolato J.-N. Thépaut F. Vitart, The ERA-Interim

465 reanalysis: configuration and performance of the data assimilation system, Q. J. R. Meteorol. Soc. 137: 553–597, 2011.

Danielczok, A. and Schröder, M.: GOME Evolution "Climate" product validation report, available at: https: //earth.esa.int/documents/700255/1525725/GOME_EVL_L3_ValRep_final/db7e72c3-044d-4236-9dee-d88405b89ef0, 2017.

Domeisen, D.I.V., C.I. Garfinkel, and A.H. Butler, The Teleconnection of El Niño Southern Oscillation to the Stratosphere, Reviews of Geophysics, 57, 5–47, 2019.

470 Feldstein, S. B., Teleconnections and ENSO: The timescale, power spectra, and climate noise properties. Journal of Climate, 13, 4430–4440, 2000.

Feldstein, S. B., and C. L. E. Frankze, Atmospheric Teleconnection Patterns, in ,Nonlinear and Stochastic Climate Dynamics', C. L. E. Franzke and T. J. O'Kane, Eds., Cambridge University Press, 54-104, 2017.

Horel, J. D., A rotated principal component analysis of the interannual variability of the Northern Hemisphere 500 mb height field. Monthly Weather Review, 109, 2080 - 2092, 1981.

Hurrell, J. W., Decadal trends in the North Atlantic Oscillation: regional temperatures and precipitation. Science, 269, 676–679, 1995.

Khaykin, S. M., Godin-Beekmann, S., Keckhut, P., Hauchecorne, A., Jumelet, J., Vernier, J.-P., Bourassa, A., Degenstein, D. A., Rieger, L. A., Bingen, C., Vanhellemont, F., Robert, C., DeLand, M., and Bhartia, P. K.: Variability and evolution of the midlatitude stratospheric aerosol budget from 22 years of ground-based lidar and satellite observations, Atmos. Chem. Phys., 17, 1829–1845, https://doi.org/10.5194/acp-17-1829-2017, 2017.

King, A. D., van Oldenborgh, G. J., & Karoly, D. J., Climate change and El Nino increase likelihood of Indonesian heat and drought, Bulletin of the American Meteorological Society, 97, S113–S117, 2016.

Nigam, S., & Baxter, S., General Circulation of the Atmosphere: Teleconnections. Encyclopedia of Atmospheric Sciences, 3, 90–109, 2015.

Simpson, J. J., J. S. Berg, C. J. Koblinsky, G. L. Hufford, and B. Beckley, The NVAP global water vapor data set: Independent crosscomparison and multiyear variability, Remote Sens. Environ., 76, 112–129, 2001.

Soden, B. J., The sensitivity of the hydrological cycle to ENSO, J. Clim., 13, 538– 549, 2000.

Thompson, D. W. J., and J. M. Wallace, The Arctic Oscillation signature in the wintertime geopotential height temperature fields. Geophysical Research Letters, 25, 1297–1300, 1998.

Van Malderen, R., Pottiaux, E., Stankunavicius, G., Beirle, S., Wagner, T., Brenot, H., and Bruyninx, C.: Interpreting the time variability of world-wide GPS and GOME/SCIAMACHY integrated water vapour retrievals, using reanalyses as auxiliary tools, Atmos. Chem. Phys. Discuss., https://doi.org/10.5194/acp-2018-1170, 2018.

Wagner, T., S. Beirle, M. Grzegorski, S. Sanghavi, U. Platt, El-Niño induced anomalies in global data sets of water vapour and cloud cover derived from GOME on ERS-2, J. Geophys. Res, 110, D15104, doi:10.1029/2005JD005972, 2005.

Walker, G. T., and E.W. Bliss, World weather V. Mem. Royal Meteorological Society, 4, 53–84, 1932.

Wallace, J.M., Gutzler, D.S., Teleconnections in the geopotential height field during the northern hemisphere winter. Monthly Weather Review 109, 784–812, 1981.

Wheeler, M. C. and H. H. Hendon, An all-season real-time multivariate MJO index: Development of an index for monitoring and prediction. *Mon. Wea. Rev.*, **132**, 1917-1932, 2004.

Woolings, T., C. Franzke, D. Hodson, B. Dong, E. Barnes, C. Raible and J. Pinto,
Contrasting interannual and multidecadal NAO variability. Climate Dynamics, 45,
539–556, 2015.

Yeh, S.-W., Cai, W., Min, S.-K., McPhaden, M. J., Dommenget, D., Dewitte, Matthew Collins , Karumuri Ashok, Soon-Il An, Bo-Young Yim, B., Kug, J.-S., ENSO atmospheric teleconnections and their response to greenhouse gas forcing. Reviews of Geophysics, 56, 185–206, 2018.

**Tables**

**Table 1: Meteorological data sets used in this study**

| Quantity | Source | Altitude |
|---|---|---|
| Water vapor VCD | Satellite observations | Total colum |
| Water vapor VCD | ECMWF reanalysis (all sky conditions) | Total colum |
| Water vapor VCD | ECMWF reanalysis (clear sky conditions) | Total colum |
| Surface temperature | ECMWF reanalysis (all sky conditions) | Surface |
| Surface pressure | ECMWF reanalysis (all sky conditions) | Surface pressure extrapolated to sea level |
| Geopotential heights | ECMWF reanalysis (all sky conditions) | 50hPa, 200hPa, 500hPa, 850hPa, 950hPa |
| Zonal winds | ECMWF reanalysis (all sky conditions) | 50hPa, 200hPa, 500hPa, 850hPa, 950hPa |
| Meridional winds | ECMWF reanalysis (all sky conditions) | 50hPa, 200hPa, 500hPa, 850hPa, 950hPa |

*the zonal winds at 50hPa are not further analysed, because they are – by definition - dominated by the QBO teleconnection signal.

**Table 2: Teleconnection indices and other time series used in this study. More details about these indices as well as their sources are given in Fig. A6 in the appendix.**

| Indices similar to ENSO (7) | Other oceanic indices (16) | Atmospheric polar indices (8) | MJO indices (15) | Other atmospheric indices (8) | Others indices (7) |
|---|---|---|---|---|---|
| BEST<br>N34<br>TPI<br>ONI<br>ENSO<br>N4<br>IND | HAW<br>PDO<br>PMM<br>N1<br>TNI<br>NTA<br>TNA<br>WHWP<br>IPO<br>CAR<br>AMO<br>DMI<br>AMM<br>STA<br>TSA<br>EA_ersst | SCA<br>AAO<br>EAWR<br>NAO<br>EPNP<br>AO<br>PE<br>WP | MJ1<br>MJ2<br>MJN<br>VPM1<br>VPM2<br>VPMN<br>RMM1<br>RMM2<br>RMMN<br>OOMI1<br>OOMI2<br>OOMIN<br>FMO1<br>FMO2<br>FMON | PNA<br>SOI<br>NOI<br>EA<br>QBO<br>Q30<br>Q50<br>Q70 | Solar indices:<br>RI<br>MGII<br>SWO<br>S107<br>AP<br><br>HUR<br>(hurricane frequency)<br><br>SAOD<br>(stratospheric AOD) |

**Table 3: Numbers of significant indices and most significant indices for all data sets (the number of indices with p99 values below threshold but shift ratios <0.8 are indicated in brackets). The complete list of significant indices for the different data sets is provided in Table A1 in the appendix.**

| Data set | Number of significant indices | Most significant index | Maximum relative significance p99 delta RMS value |
|---|---|---|---|
| TCWV sat | 42 (2) | ONI | 9.9 |
| TCWV ERA | 44 (1) | ONI | 12.6 |
| TCWV ERA clear | 42 (3) | ONI | 11.6 |
| Tsurf (surface temperature) | 37 (1) | ONI | 6.6 |
| Spred (surface pressure) | 35 (1) | AAO | 19.1 |
| Geopot 50 hPa | 17 (5) | AAO | 8.7 |
| Geopot 200 hPa | 40 (0) | AAO | 23.3 |
| Geopot 500 hPa | 32 (1) | AAO | 21.4 |
| Geopot 850 hPa | 33 (1) | AAO | 20.2 |
| Geopot 950 hPa | 30 (1) | AAO | 19.0 |
| Zonal winds 200 hPa | 51 (0) | BEST | 15.0 |
| Zonal winds 500 hPa | 49 (0) | BEST | 7.2 |
| Zonal winds 850 hPa | 46 (1) | BEST | 11.0 |
| Zonal winds 950 hPa | 42 (4) | AO | 11.8 |
| Meridional winds 50 hPa | 24 (3) | AAO | 2.9 |
| Meridional winds 200 hPa | 32 (1) | AAO | 5.4 |
| Meridional winds 500 hPa | 34 (0) | AAO | 4.5 |
| Meridional winds 850 hPa | 33 (0) | SCA | 6.1 |
| Meridional winds 950 hPa | 32 (0) | SCA | 6.0 |

550

555

560

565

570

575

580

585

590

**Figures**
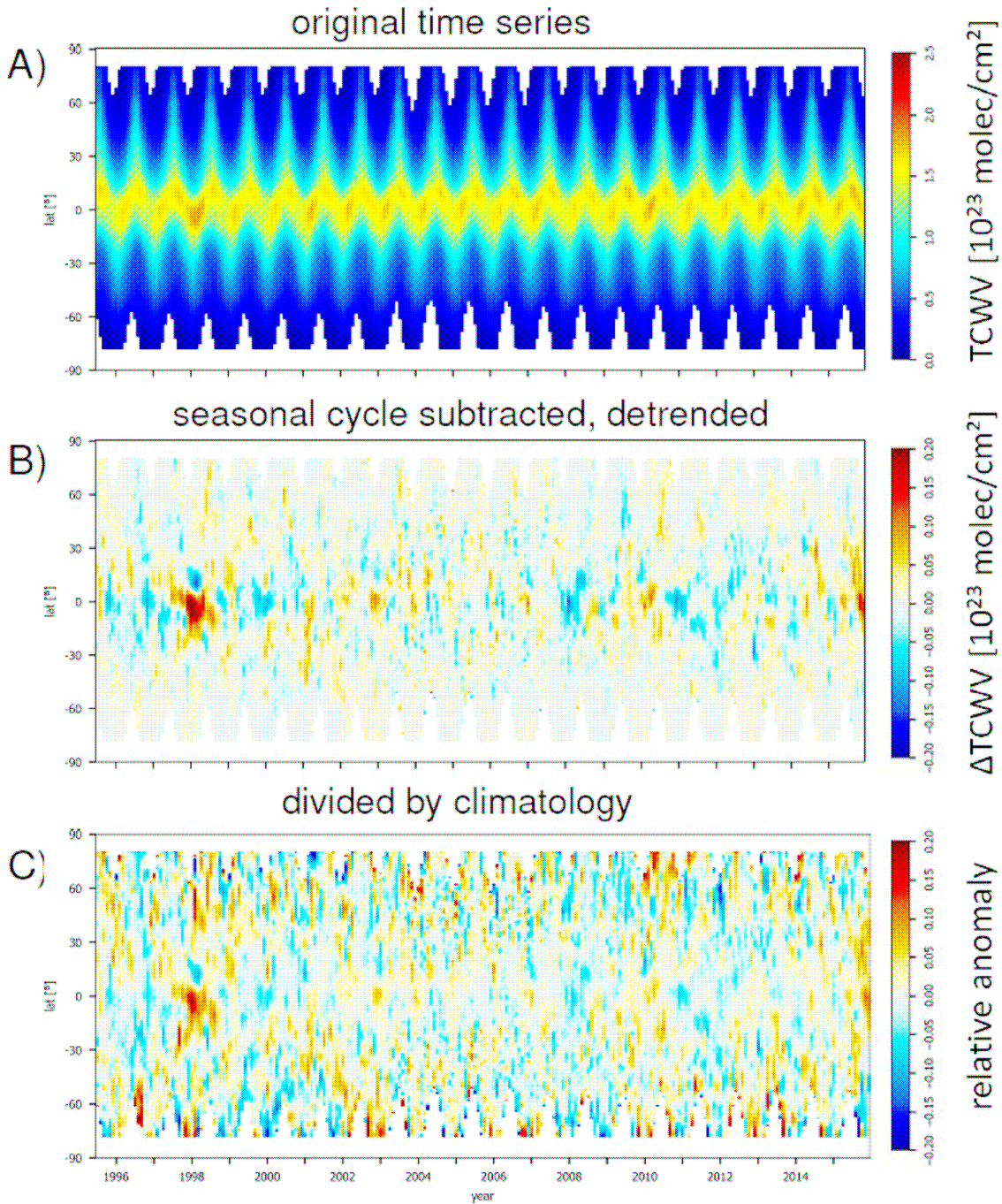
Fig. 1: A) TCWV measured from satellite as a function of time and latitude (zonally averaged values) on a 1° x 1° latitude/longitude grid with monthly resolution. B) (absolute anomalies) after the mean seasonal cycle and a linear trend was subtracted. C) relative anomalies (absolute anomalies divided by the corresponding monthly mean TCWV).

595

600

605

610
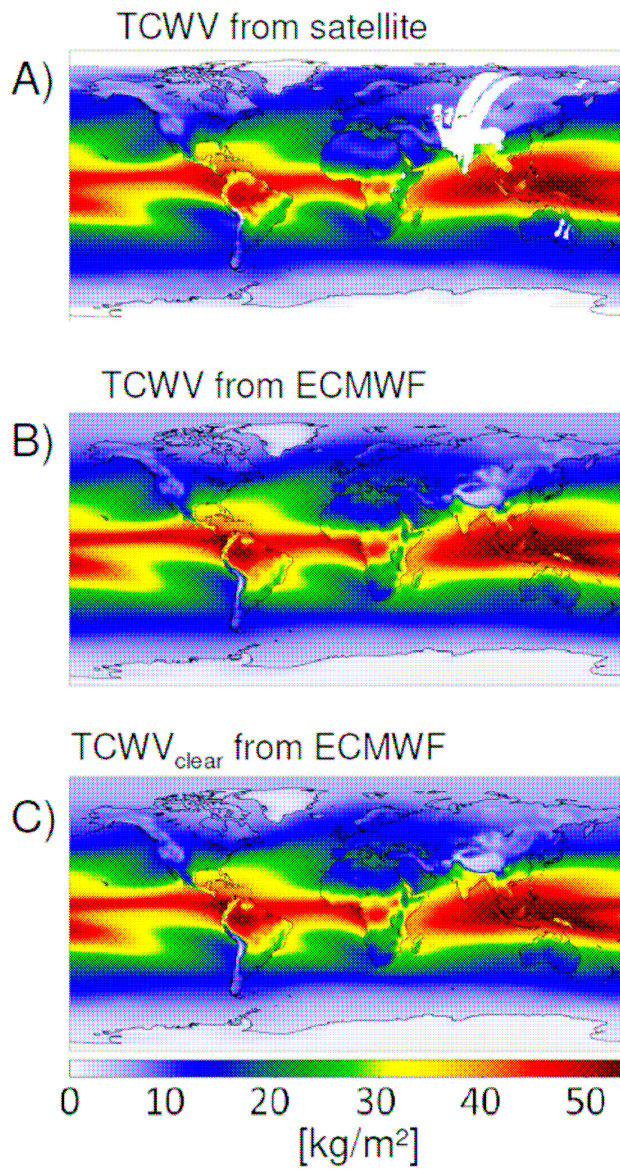
**Fig. 2: Global mean distribution of the TCWV from satellite observations (A) and ERA data: B) all data; C) only clear sky observations during day.**

640
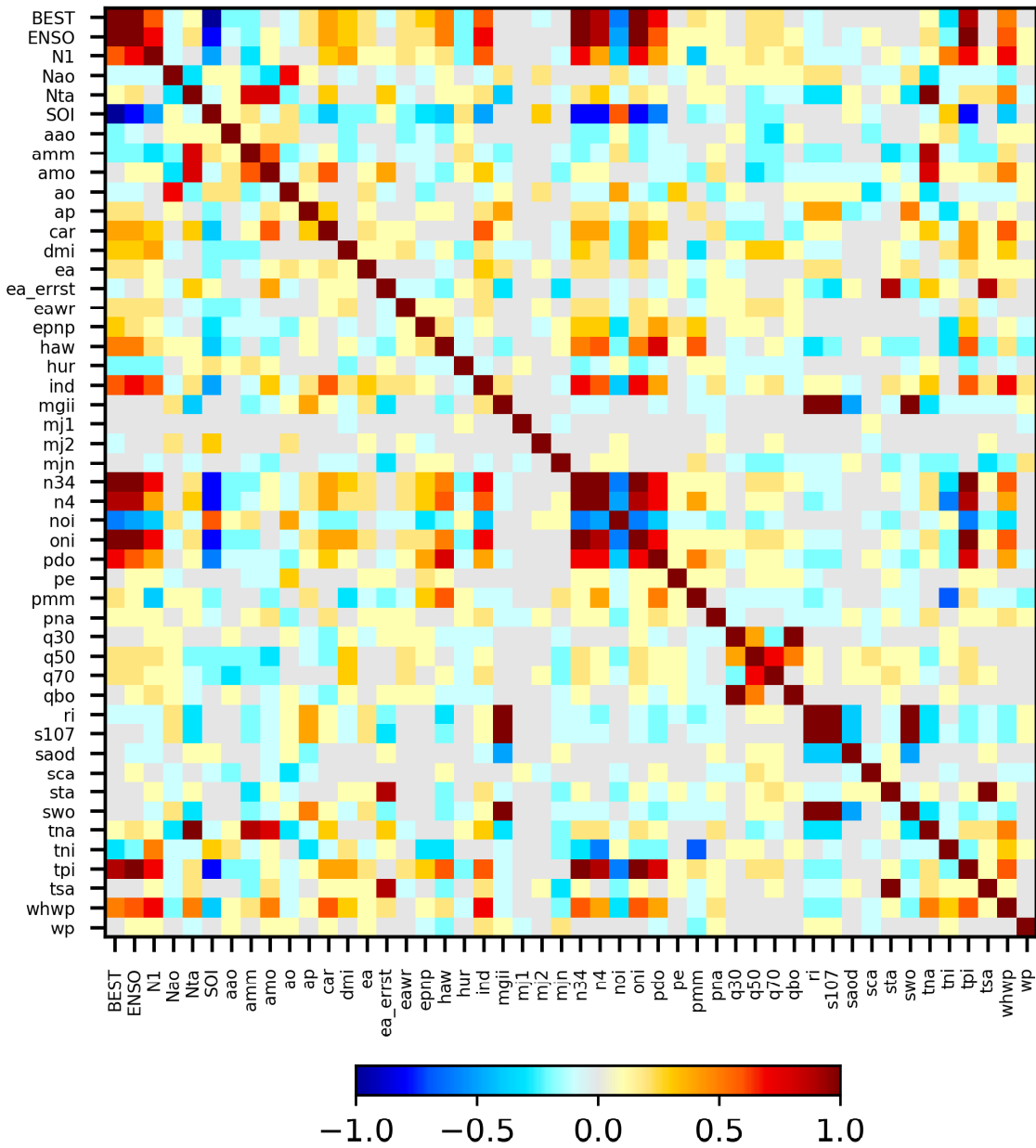
**Fig. 3: Correlation coefficients between the different teleconnection indices (after seasonal cycle was removed). Note that only one set of MJO indices is included here to minimise the total number of indices.**

645

650

655

660

665
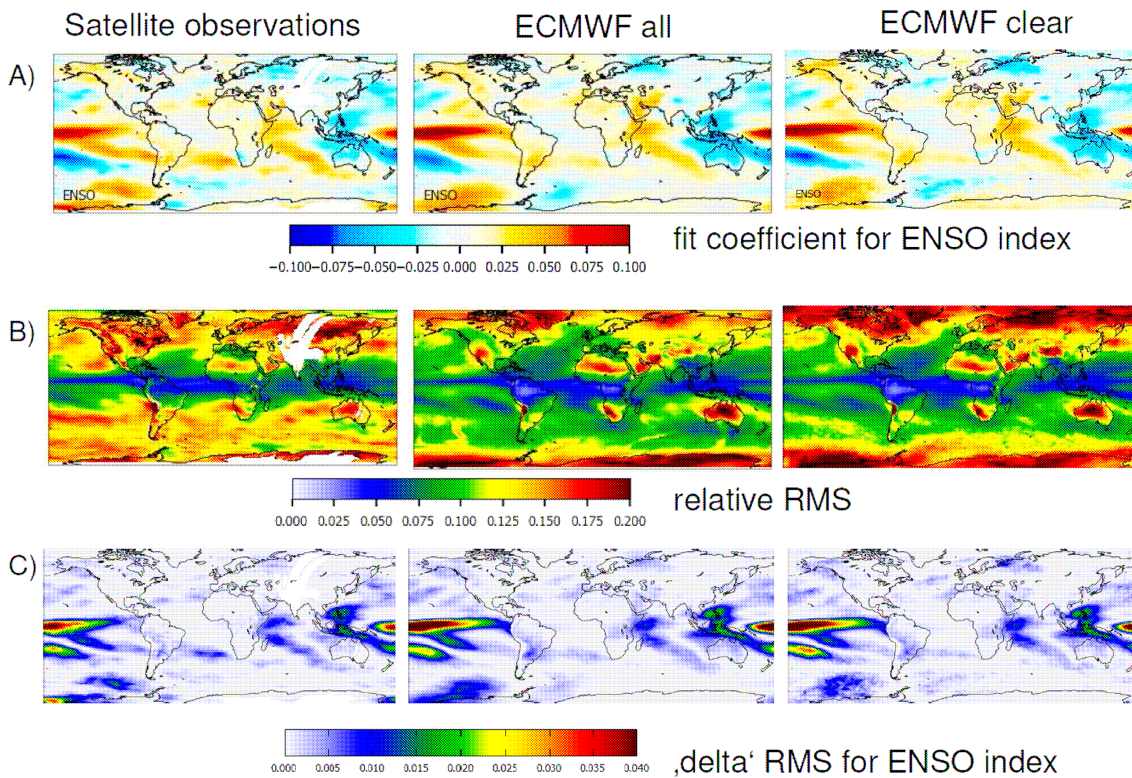
Fig. 4: Global maps with the ENSO fit results for the three TCWV data sets. A) Fit coefficients; B) RMS of the differences between original data sets and fit functions; C) delta RMS values which describe the relative difference of the RMS if the ENSO index is included or excluded in the fit function (for details see text).

670

675

680

685

690

695

700
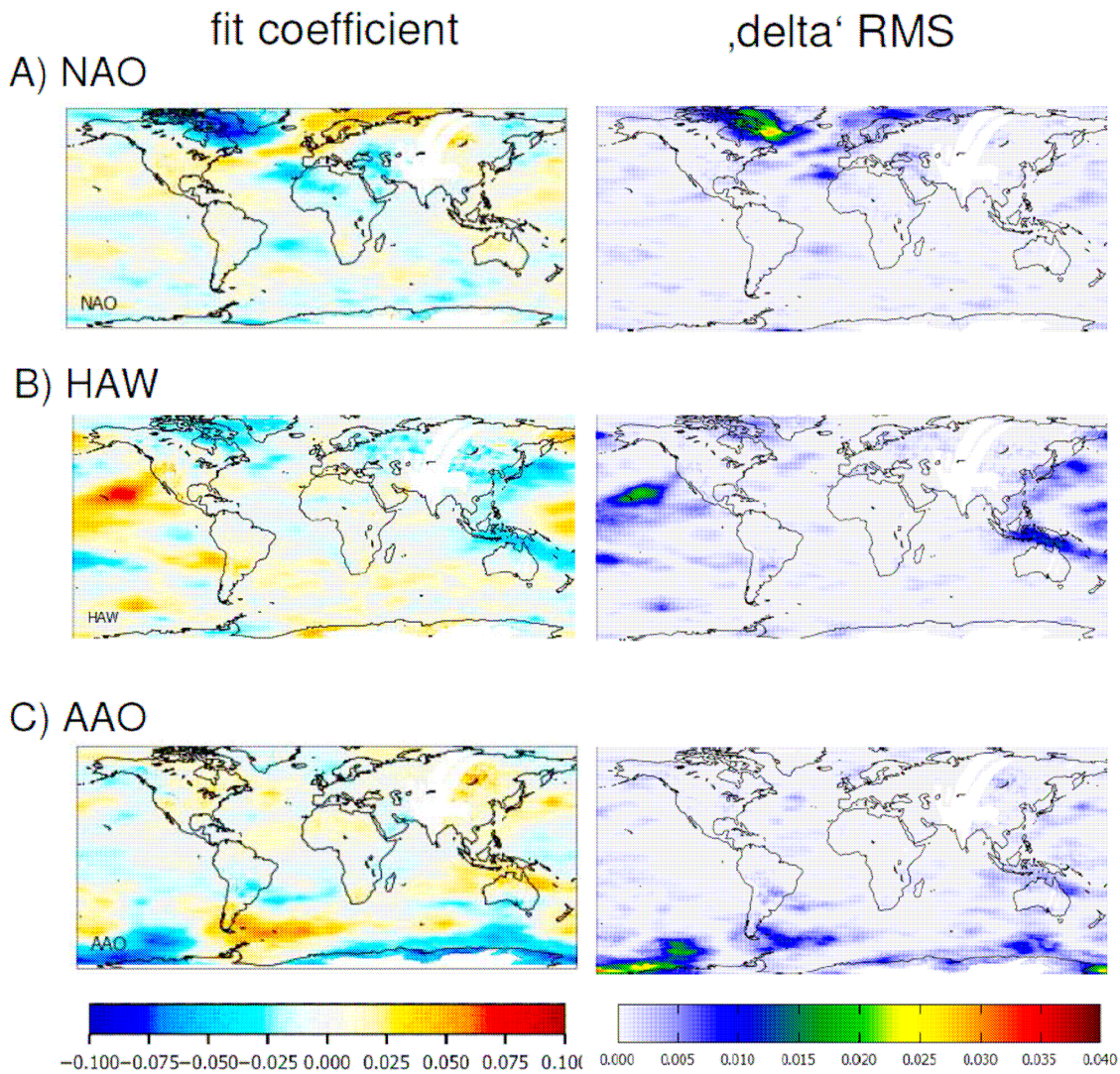
**Fig. 5: Global maps with the fit results (right) and delta RMS (left) for selected teleconnection indices with activity centers in northern high latitudes (A), Subtropics (B) and southern high latitudes (C). Results for the TCWV data set from satellite observations.**
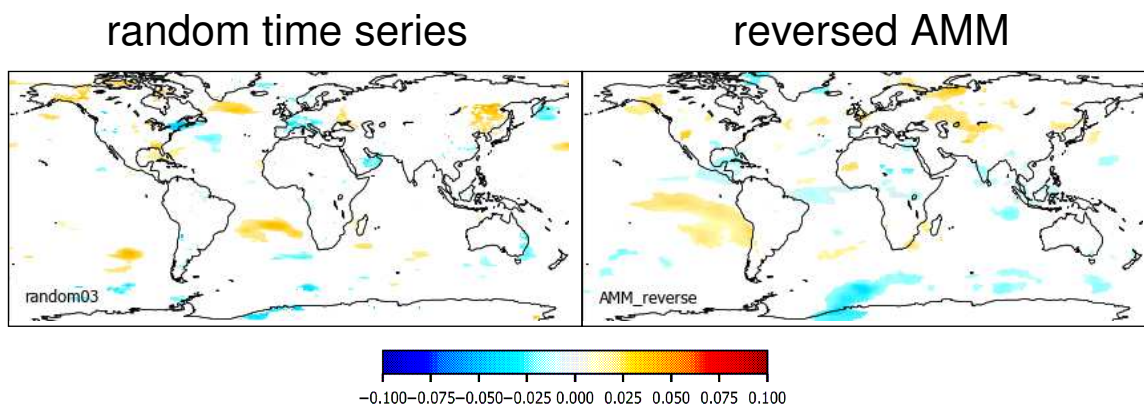
**Fig. 6 Global maps of the fit results for an artificial time series containing only white noise (left) and a temporally reversed teleconnection index (AMM, right). The white areas represent fit results, that are classified as non-significant by the fit routine (for a 5% significance level).**

720
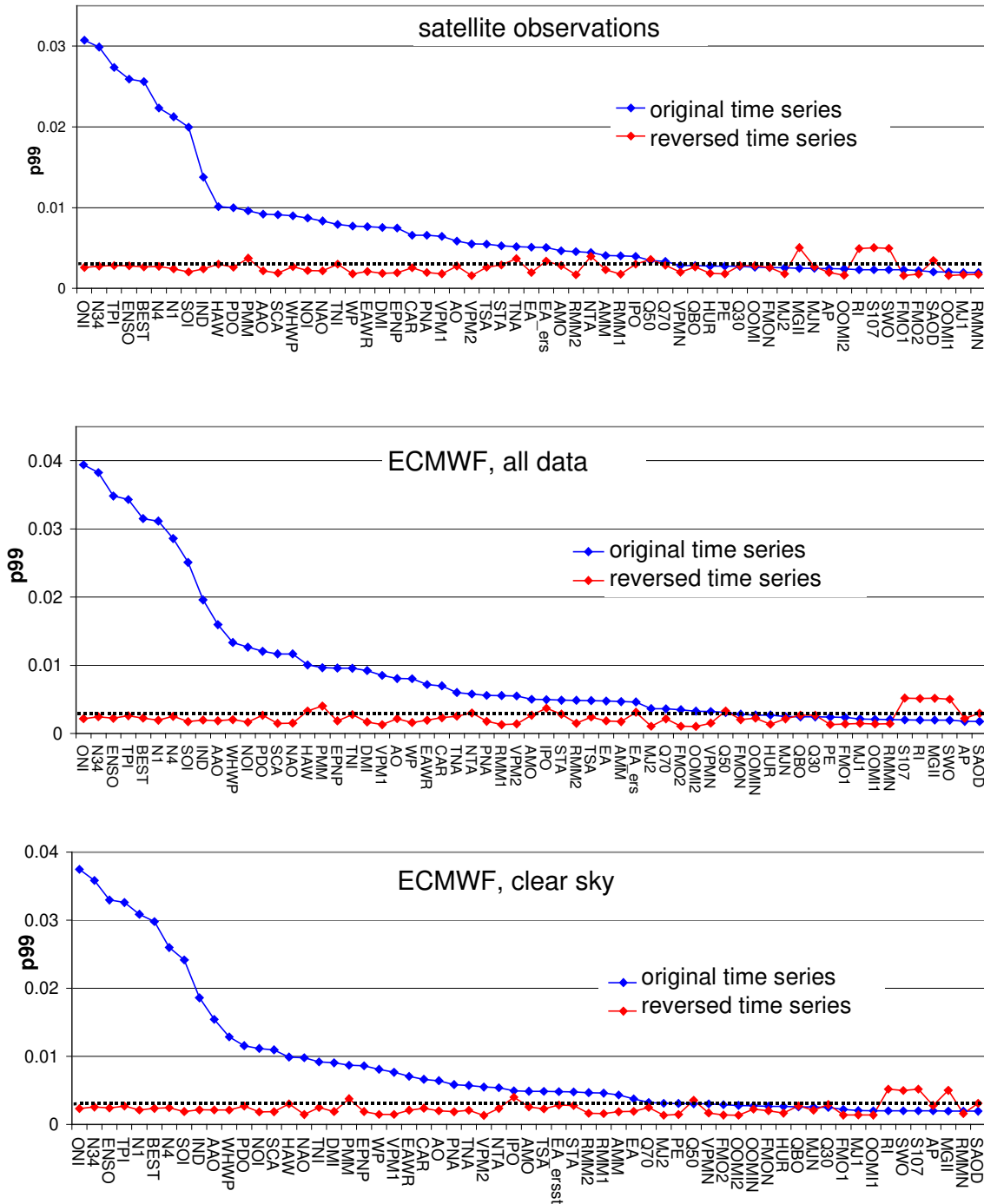
**Fig. 7: Blue markers: 99th percentiles (p99) of the delta RMS of the original indices for the three TCWV data sets. Red markers: similar results for the temporally reversed indices. Black lines: significance threshold. The indices are sorted from highest to lowest p99 values for the original indices.**

730

735
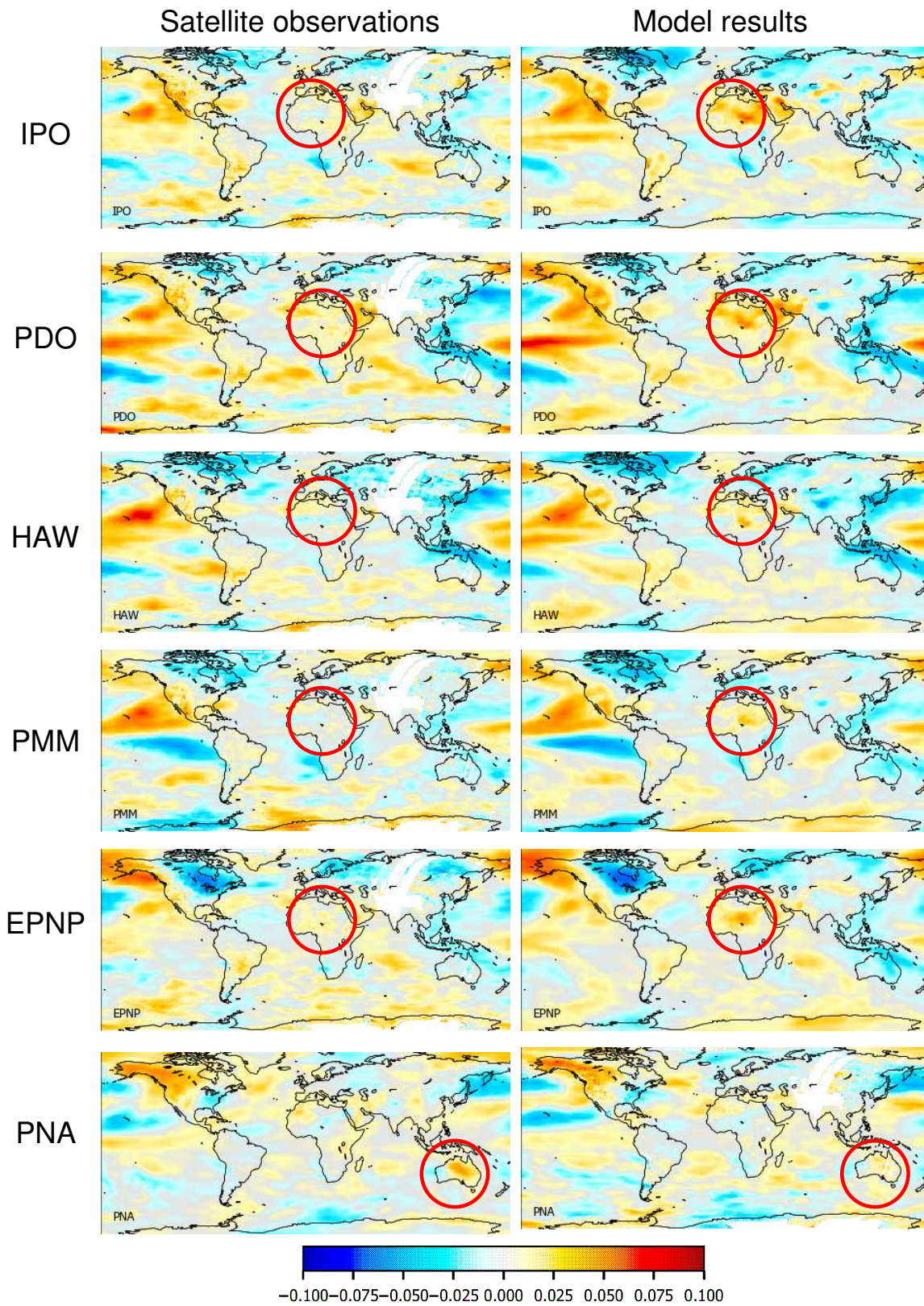
**Fig. 8: Fit coefficients for selected teleconnection indices, for which different patterns were found in the TCWV data set from satellite observations (left) and model simulations (right). The red circles indicate regions with substantial differences between the results for both data sets.**
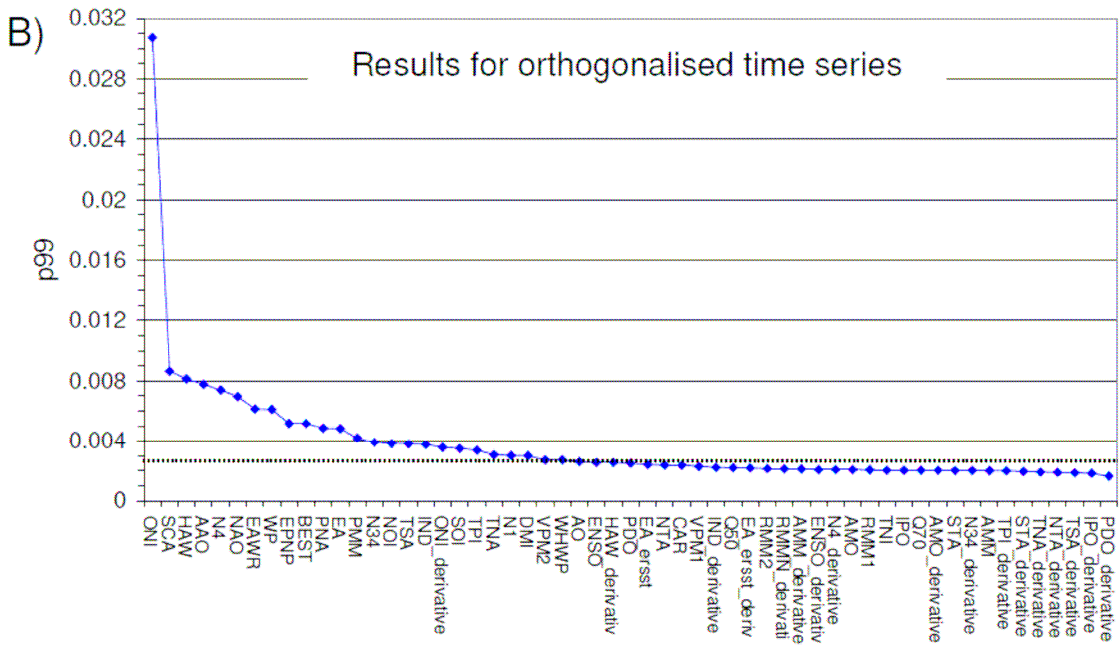
**Fig. 9. The 99th percentiles (p99) of the delta RMS of the orthogonalised indices. The black lines represent the significance threshold. The indices are sorted from highest to lowest p99 values.**

A) Significant original indices satellite
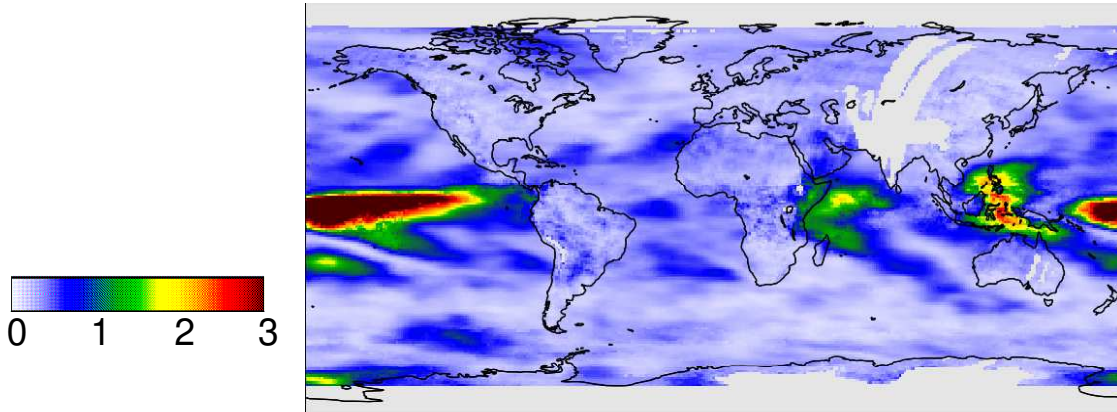
B) Significant orthogonalised indices satellite
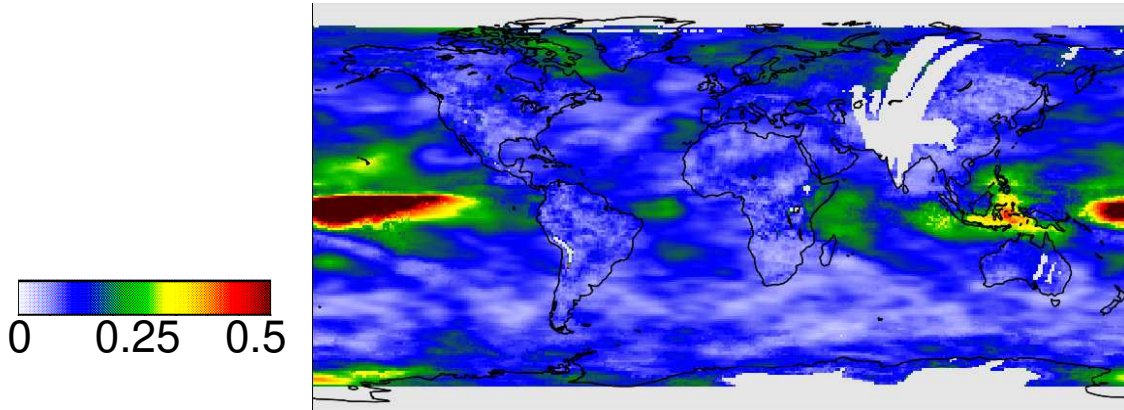
C) Significant orthogonalised indices ECMWF
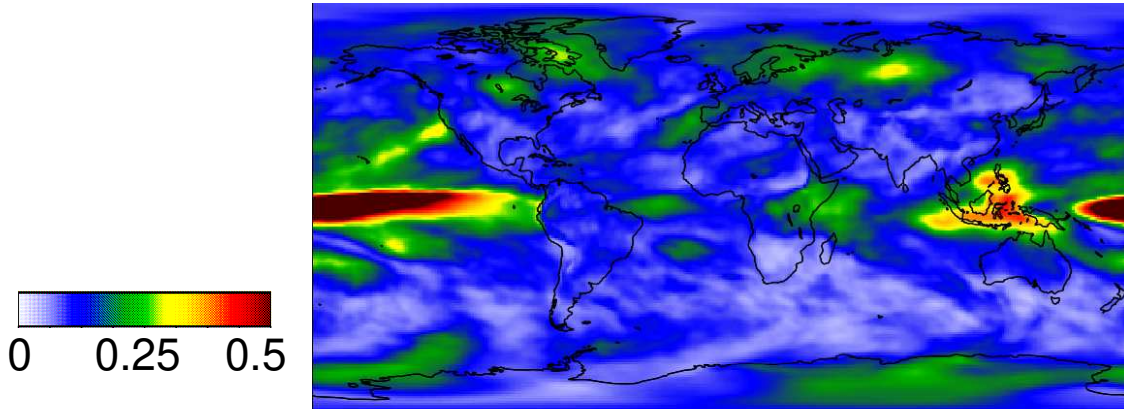
775

**Fig. 10: Cumulative delta RMS for different selections of indices and data sets (note the different colour scales).**

780

785

790

795
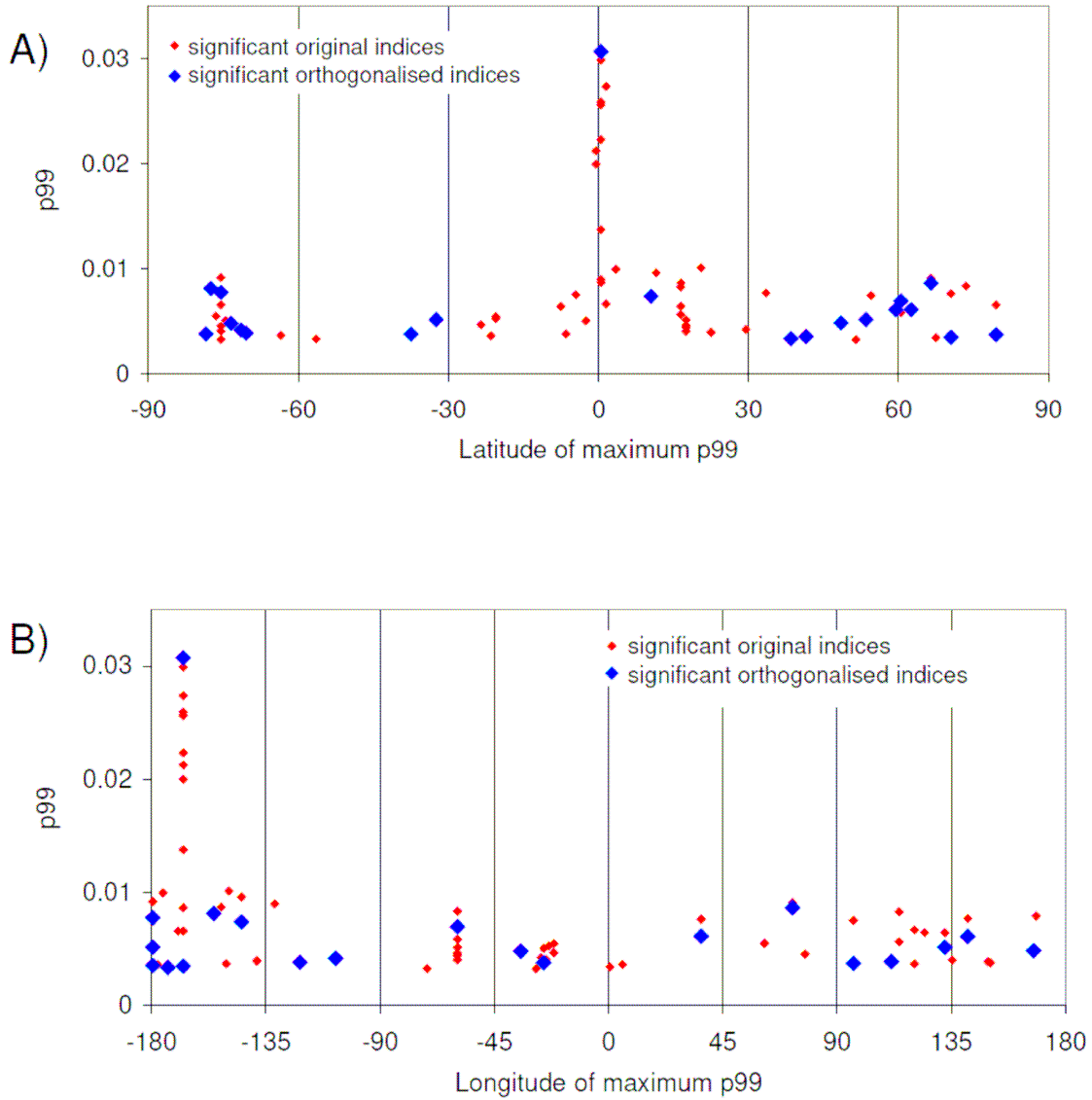
Fig. 11: Location of the 99th percentile of the delta RMS values detected in the TCWV data derived from satellite observations as function of latitude (A) or longitude (B). Red points indicate results for the original indices, blue points for the orthogonalised indices.

800

805

810

815

**Appendix 1**

**Normalisation of the delta RMS values**

In many teleconnection studies (e.g. Horel, 1981 and references therein), the strength of a teleconnection index is quantified by calculating the ratio of the difference of the RMS (with and without an index included) and the total RMS. In this study we applied a different procedure, because the total RMS depends on many factors, in particular also on the uncertainties of the considered data set. Since we want to compare the delta RMS values derived for different data sets (in particular the TCWV data sets derived from satellite observations and model results, but also other datasets) in a quantitative way, we decided to divide the RMS (with and without an index included) by the zonal mean of the considered data set. Thus the delta RMS shows the relative impact of the respective index. While the RMS of the different TCWV data sets are rather different (see Fig. 4, middle panel), the zonal means are very similar (Fig. 2). The zonal mean was chosen (instead of the long term average of each considered 1° x 1° pixel), because for some data sets used in this study (especially the wind data sets) large variations and even zero-crossings exist, which would lead to meaningless delta-RMS values. We compared the delta RMS values calculated by our new definition with those of the more traditional definition for the TCWV data sets (Fig. A1). The obtained global patterns of both delta RMS definitions are almost identical.
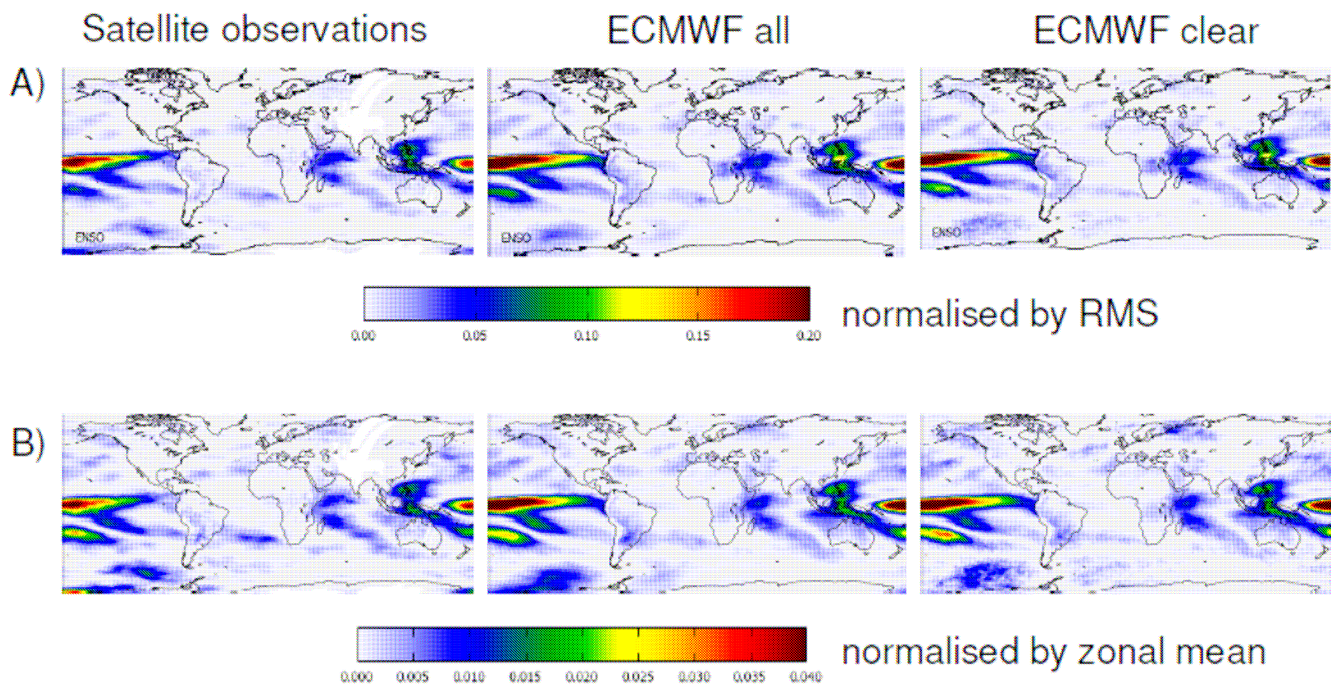
Fig. A1: Comparison of delta RMS values for the ENSO index calculated in two different ways. A) The difference of the RMS with and without the ENSO index included in the fit is divided by the respective RMS of each 1°x1° pixel; B) The difference of the RMS with and without the ENSO index included in the fit is divided by the zonal mean of the TCWV at the same latitude. Note the different colour scales.

**Appendix 2**

**Effect of the temporal correlation of the reversed indices with the original indices**

For several temporally reversed indices, the 99th percentiles in Fig. 7 are substantially higher than for others. Since all reversed indices represent non-geophysical variations, such enhanced 99th percentiles are not expected. Thus this finding was further investigated. It turned out that the enhanced values are caused by accidental correlations of these reversed indices with original indices (see Fig. A2), for which high 99th percentile values are found. This reasoning is confirmed by the results shown in Fig. A3. There, high p99 values for reversed indices are always found if they are correlated with original indices with high p99 values. To avoid the effects of such accidental enhanced p99 values, only the reversed indices with no obvious correlations with original indices with high p99 values were kept for further processing (red boxes in Fig. A3). Here it should be noted that two somehow arbitrary choices were made:

a) the selection of the selected reversed indices (red boxes in Fig. A3) was made by visual inspection.

b) the effect of the correlation of the reversed indices with the original indices was only investigated for the 8 original indices with the highest p99 values.

Fortunately, both choices had only a minor influence on the derived threshold value. With respect to the first point, it should be noted that while the selection was made rather conservatively, still many reversed indices were kept after the filtering process. It was also found that most of the skipped reversed indices were removed because of enhanced correlations with several original indices. With respect to the second point it should be noted that it makes sense to consider only the original indices with the highest p99 values, because the correlations of the reversed indices with the original indices are in general rather low (see Fig. A2). The p99 values of the selected 8 original indices with the highest p99 values are in general substantially higher than the p99 values of the remaining indices. In sensitivity studies we found that taking account more than 8 original indices had a negligible effect on the derived threshold values.

The red markers in Fig. A4 represent the p99 values for the indices which were kept after applying the selection criteria explained above. In the final step, from these p99 values the average and standard deviation are calculated. The p99 threshold for the significance of a indices is then calculated as the sum of the average plus three times the standard deviation (for the TCWV data set from satellite observations the threshold is: $0.00200 + 3*0.00036 = 0.00309$). This procedure was chosen, because the threshold values calculated in this way are very close to the maximum p99 values of the remaining indices (red dots in Fig. A4) but are hardly affected by possible remaining outliers. The derived threshold value is indicated by the dashed black line in Fig. 7.
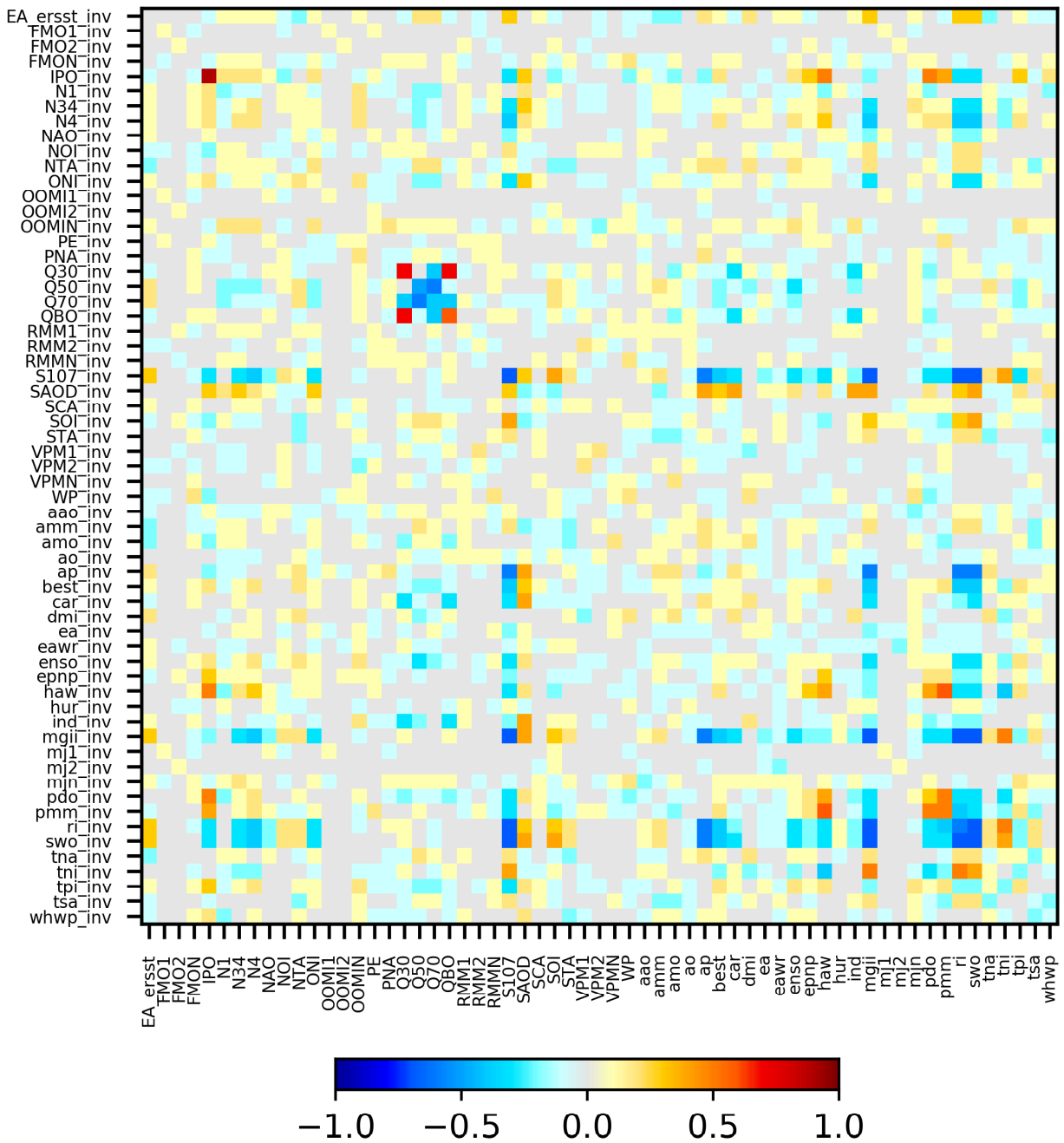
**Fig. A2: Correlation coefficients between the temporally reversed and original indices. For several combinations enhanced coincidental correlations are found.**
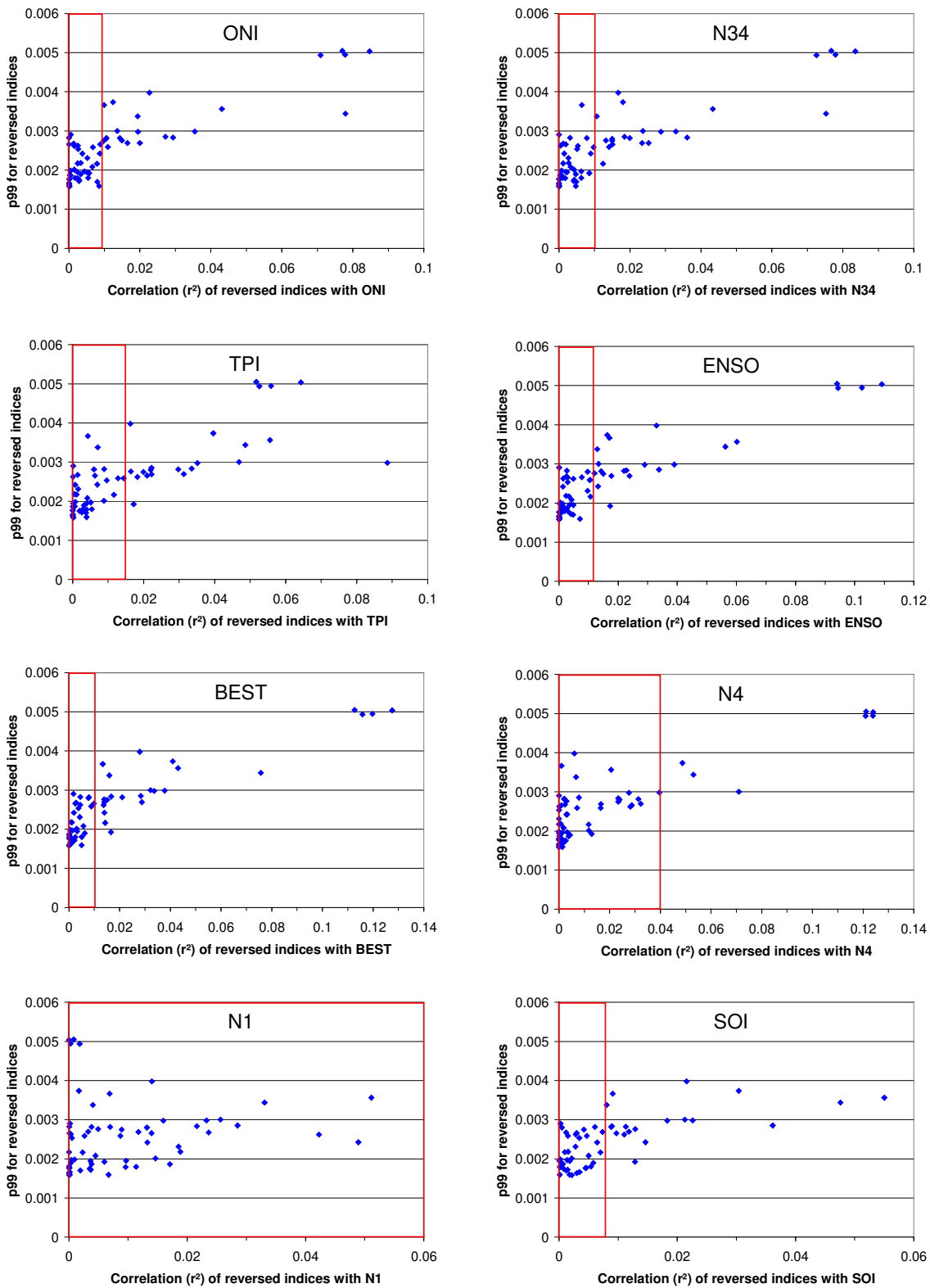
895

**Fig. A3: Correlation plots for the 8 original indices with the highest p99 values. The blue dots represent the 61 reversed indices. The x-axis describes the correlation coefficients of the reversed indices with the selected original indices. The y-axis describes the p99 value or the reversed indices. High p99 values are found for the reversed indices which show high correlation to the original indices.**

900
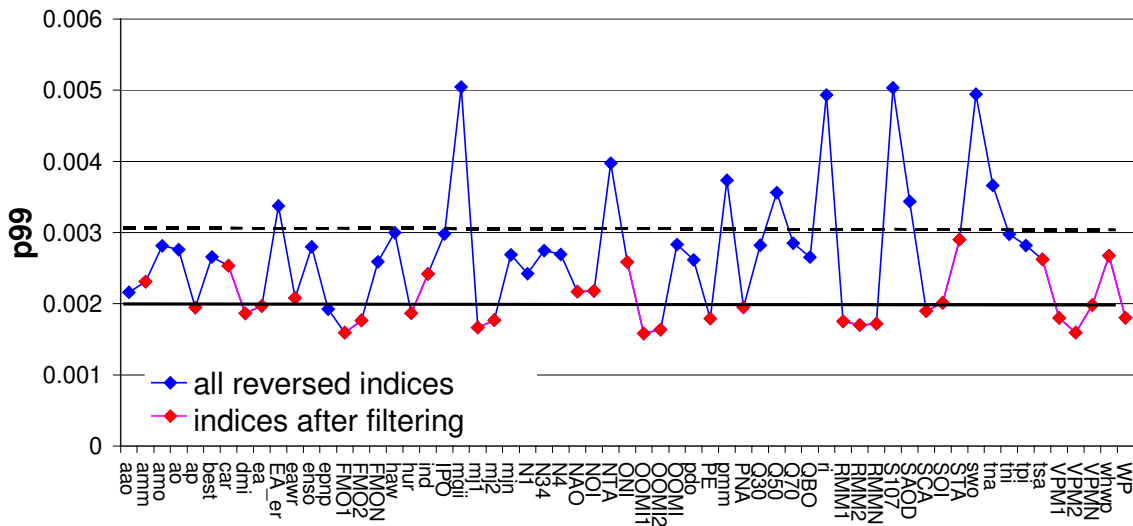
905

**Fig. A4: The 99th percentiles (p99) of the delta RMS of the temporally reversed indices for the TCWV from satellite observations (same as in Fig. 7, top). The blue markers indicate indices which are excluded from the calculation of the significance threshold (for details see text).**

910

915 **Appendix A3**

**Effect of a time shift of the teleconnection indices**

In addition to the p99 values themselves, also the effect of time shifts Δt = ± 1 month of the indices on the p99 values was considered to decide whether an index was significantly identified in a global data set, because for indices with a geophysical relationship to a considered data set, the exact temporal synchronisation should be important (but might depend on region).

920 In contrast, for indices without a geophysical relationship to the considered data set, the p99 values should not depend on the exact temporal synchronisation. Here it should be noted that for some teleconnections, also time lags might exist between the corresponding indices and the atmospheric variables. Thus the lack of an exact synchronization should not be seen as a strong indication that the corresponding teleconnection was not significantly detected in a global data set. But conversely, if a clear synchronisation for a teleconnection is found, this can be interpreted as a a strong indication for significant detection.

925 In Fig. A5 the p99 values for the original and shifted (by ± 1 month) indices are shown for the TCWV data set from satellite observations. For most data sets (especially for those with high p99 values) indeed smaller p99 values are found for the shifted indices. Here it is interesting to note that in general a stronger effect is found for atmospheric indices than for oceanic indices, which can be understood by the higher frequencies of the atmospheric indices. For several oceanic indices, even higher values are found for the shifted indices indicating a time shift (mostly a time lag) between the TCWV and these

930 indices. For one index (AMM) higher p99 values are even found for shifts in both directions indicating an ambiguity in the synchronisation between the TCWV and the AMM index.

Another interesting finding is that for some atmospheric indices with p99 values below the significance threshold (PE, MJ2, OOMI2, FMO1) still rather small ratios of the shifted and original indices are found indicating that these indices are also probably significantly detected in the TCWV data set. Thus in the following we consider also indices with p99 values below

935 the significance threshold but with p99 ratios below 0.8 for both shifts as significantly detected. Here it should be noted that the choice of the threshold value of 0.8 is somehow arbitrary. It was chosen because a deviation of 20% from unity is larger than the 'noise level' of the ratio. The exact choice of the threshold has only a small effect on the obtained results.
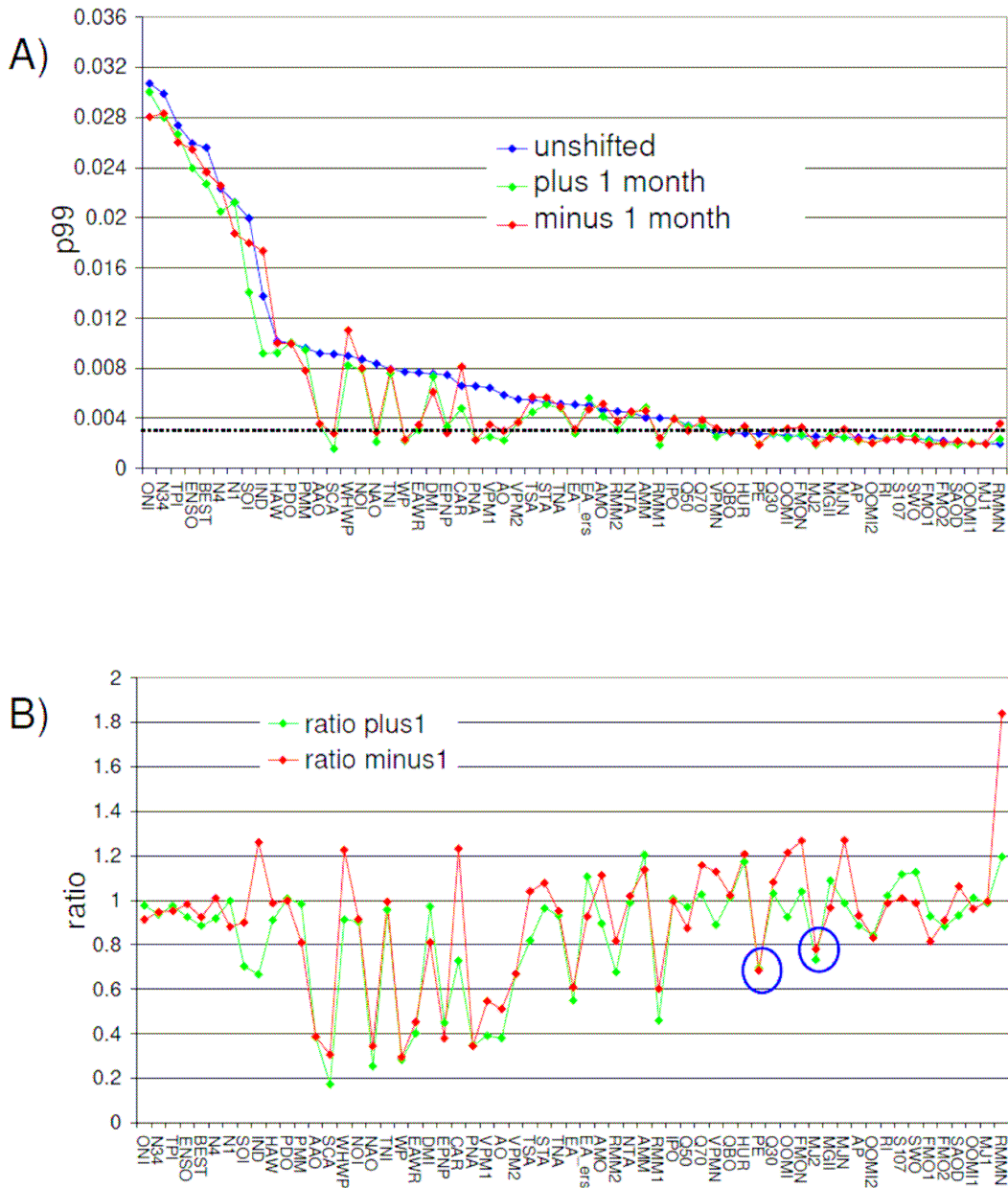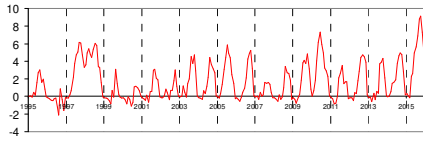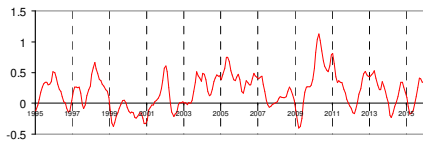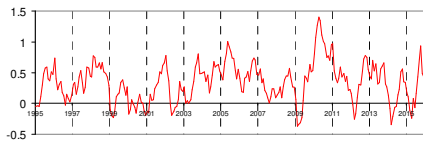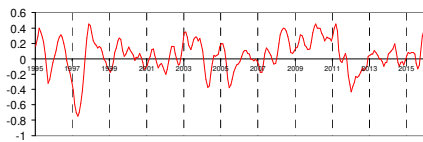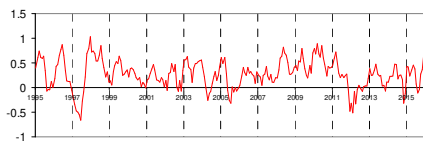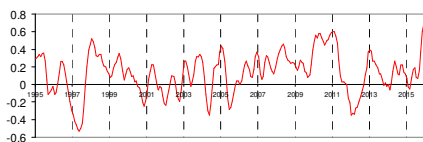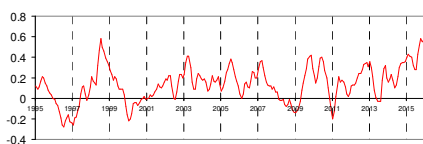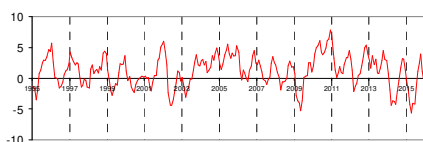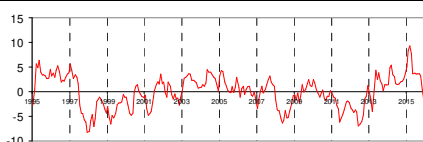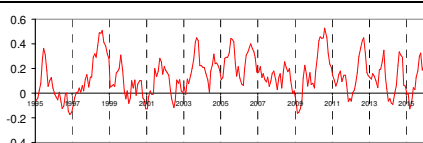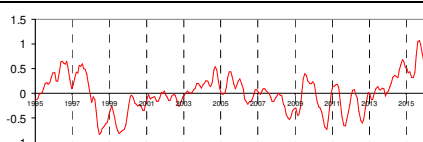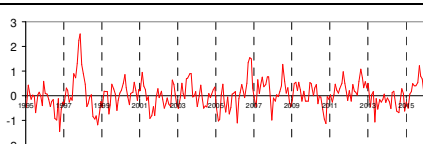
**Fig. A5: Top: 99th percentiles (p99) of the delta RMS values for the original (blue) and shifted indices (green: plus 1 month; red: minus 1 month). The indices are sorted from highest to lowest p99 values for the unshifted original indices. Bottom: ratios of the p99 values of the shifted and original indices. Results are for the TCWV data set from satellite observations. The blue circles indicate teleconnection indices with p99 values below the threshold, but ratios of the shifted indices < 0.8.**

940

945

950

955

960

**Appendix 4**

 **Additional Figures and tables**
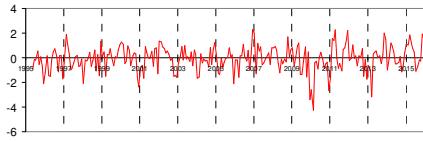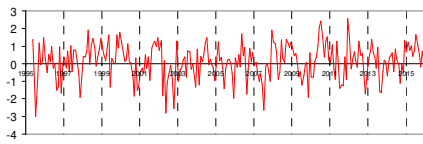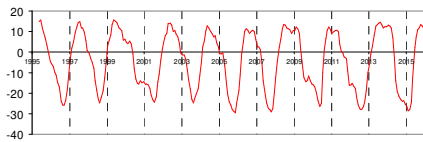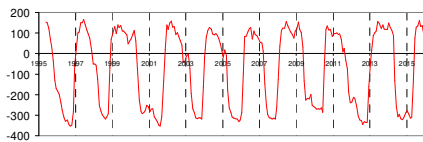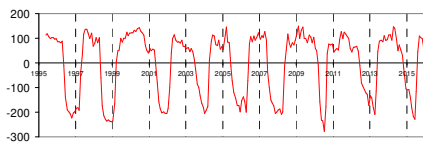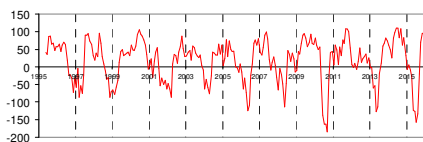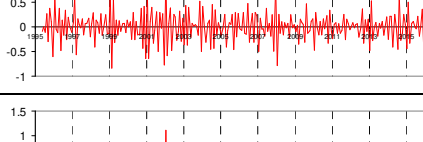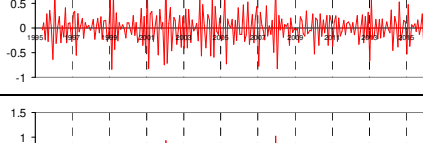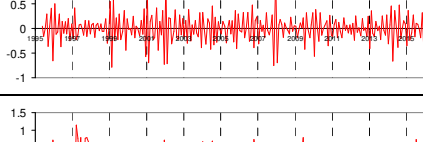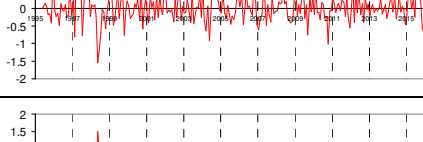
| Name (data source) | Short name | Type | Indices 1995 - 2015 |
|---|---|---|---|
| **A) Indices similar to ENSO** | | | |
| Multivariate ENSO Index (NOAA) | ENSO | Oceanic & Atmospheric | |
| Bivariate ENSO Timeseries (NOAA) | BEST | Oceanic & Atmospheric | |
| Oceanic Nino Index (NOAA) | ONI | Oceanic | |
| Nina 3.4 (NOAA) | N34 | Oceanic | |
| Nina 4 (NOAA) | N4 | Oceanic | |
| Tripole Index for the Interdecadal Pacific Oscillation (NOAA) | TPI | Oceanic | |
| Indian Ocean Index (NOAA) | IND | Oceanic | |
| | | | |
| **B) Oceanic indices** | | | |
| Nina 1 + 2 (NOAA) | N1 | Oceanic | |
| Pacific Decadal Oscillation (NOAA) | PDO | Oceanic | |
| Interdecadal Pacific Oscillation (Ministry of environment, NZ) | IPO | Oceanic | |

| | | | |
|---|---|---|---|
| Western Hemisphere warm pool (NOAA) | WHWP | Oceanic |  |
| North Tropical Atlantic (NOAA) | NTA | Oceanic |  |
| Tropical Northern Atlantic (NOAA) | TNA | Oceanic |  |
| South Tropical Atlantic (NOAA) | STA | Oceanic |  |
| Tropical Southern Atlantic (NOAA) | TSA | Oceanic |  |
| Equatorial Atlantic Index (NOAA) | EA_ersst | Oceanic |  |
| Caribbean Index (NOAA) | CAR | Oceanic |  |
| Atlantic Meridional Mode (NOAA) | AMM | Oceanic |  |
| Pacific Meridional mode (University of Wisconsin, USA) | PMM | Oceanic |  |
| Atlantic multidecadal Oscillation (NOAA) | AMO | Oceanic |  |
| Hawaiian Index (NOAA) | HAW | Oceanic |  |
| Dipole Mode Index (NOAA) | DMI | Oceanic |  |

| Trans-Nino index (NOAA) | TNI | Oceanic |  |
|---|---|---|---|
| | | | |
| **C) Atmospheric indices (except MJO indices)** | | | |
| Southern Oscillation Index (NOAA) | SOI | Atmospheric |  |
| Northern Oscillation Index (NOAA) | NOI | Atmospheric |  |
| North Atlantic Oscillation (NOAA) | NAO | Atmospheric |  |
| Pacific/North American pattern (NOAA) | PNA | Atmospheric |  |
| East Atlantic pattern (NOAA) | EA | Atmospheric |  |
| East Atlantic/Western Russia pattern (NOAA) | EAWR | Atmospheric |  |
| Scandinavia pattern (NOAA) | SCA | Atmospheric |  |
| West Pacific pattern (NOAA) | WP | Atmospheric |  |
| East Pacific/North Pacific pattern (NOAA) | EPNP | Atmospheric |  |
| Polar-Eurasian pattern (NOAA) | PE | Atmospheric |  |

| Arctic Oscillation (NOAA) | AO | Atmospheric | |
|---|---|---|---|
| Antarctic Oscillation (NOAA) | AAO | Atmospheric | |
| Quasi-Biennial Oscillation at 30 hPa (NOAA) | QBO | Atmospheric | |
| Quasi-Biennial Oscillation at 30 hPa (Free University of Berlin) | Q30 | Atmospheric | |
| uasi-Biennial Oscillation at 50 hPa (Free University of Berlin) | Q50 | Atmospheric | |
| uasi-Biennial Oscillation at 70 hPa (Free University of Berlin) | Q70 | Atmospheric | |
| | | | |
| **D) MJO Indices*** | | | |
| Madden Julian Oscillation (OMI) Component 1 (NOAA) | MJ1 | Atmospheric | |
| Madden Julian Oscillation (OOMI) Component 1 (NOAA) | OOMI1 | Atmospheric | |
| Madden Julian Oscillation (FMO) Component 1 (NOAA) | FMO1 | Atmospheric | |
| Madden Julian Oscillation (VPM) Component 1 (NOAA) | VPM1 | Atmospheric | |
| Madden Julian Oscillation** Component 1 (Australian Bureau of Meteorology) | RMM1 | Atmospheric | |

| | | | |
|---|---|---|---|
| Madden Julian Oscillation (OMI) Component 2 (NOAA) | MJ2 | Atmospheric | |
| Madden Julian Oscillation (OOMI) Component 2 (NOAA) | OOMI2 | Atmospheric | |
| Madden Julian Oscillation (FMO) Component 2 (NOAA) | FMO2 | Atmospheric | |
| Madden Julian Oscillation (VPM) Component 2 (NOAA) | VPM2 | Atmospheric | |
| Madden Julian Oscillation** Component 2 (Australian Bureau of Meteorology) | RMM2 | Atmospheric | |
| Madden Julian Oscillation (OMI) Sum of both compoenents (NOAA) | MJN | Atmospheric | |
| Madden Julian Oscillation (OOMI) Sum of both (NOAA) | OOMIN | Atmospheric | |
| Madden Julian Oscillation (FMO) Sum of both (NOAA) | FMON | Atmospheric | |
| Madden Julian Oscillation (VPM) Sum of both (NOAA) | VPMN | Atmospheric | |
| Madden Julian Oscillation** Sum of both (Australian Bureau of Meteorology) | RMMN | Atmospheric | |
| | | | |
| **E) Other Indices** | | | |
| | | | |
| Composite MG II index (University of Bremen) | MGII | solar | |

| | | | |
|---|---|---|---|
| Magnetic AP index (NOAA, GeoForschungsZentrum, Postdam) | AP | solar |  |
| Radio flux at 10.7 cm (NOAA, Penticton, B.C., Canada) | S107 | solar |  |
| Sun spot number (NOAA, SWPC Space Weather Operations) | SWO | solar |  |
| Sun spot number (NOAA, S.I.D.C. Brussels International Sunspot Number) | RI | solar |  |
| **Stratospheric AOD\*\*\* (LATMOS/IPSL)** | SAOD | Atmospheric |  |
| **Total number of hurricanes in Atlantic region (NOAA)** | HUR | Atmospheric |  |

**Fig. A6: List of original indices used in this study. Besides the short names also the data sources and their temporal variation from 1995 to 2016 are shown.**

970 \*All MJO indices are convoluted with a Gaussian kernel of 30 days FWHM; \*\*Original index according to Wheeler and Hendon, 2004;
\*\*\*Khaykin et al., 2017

975

980

985
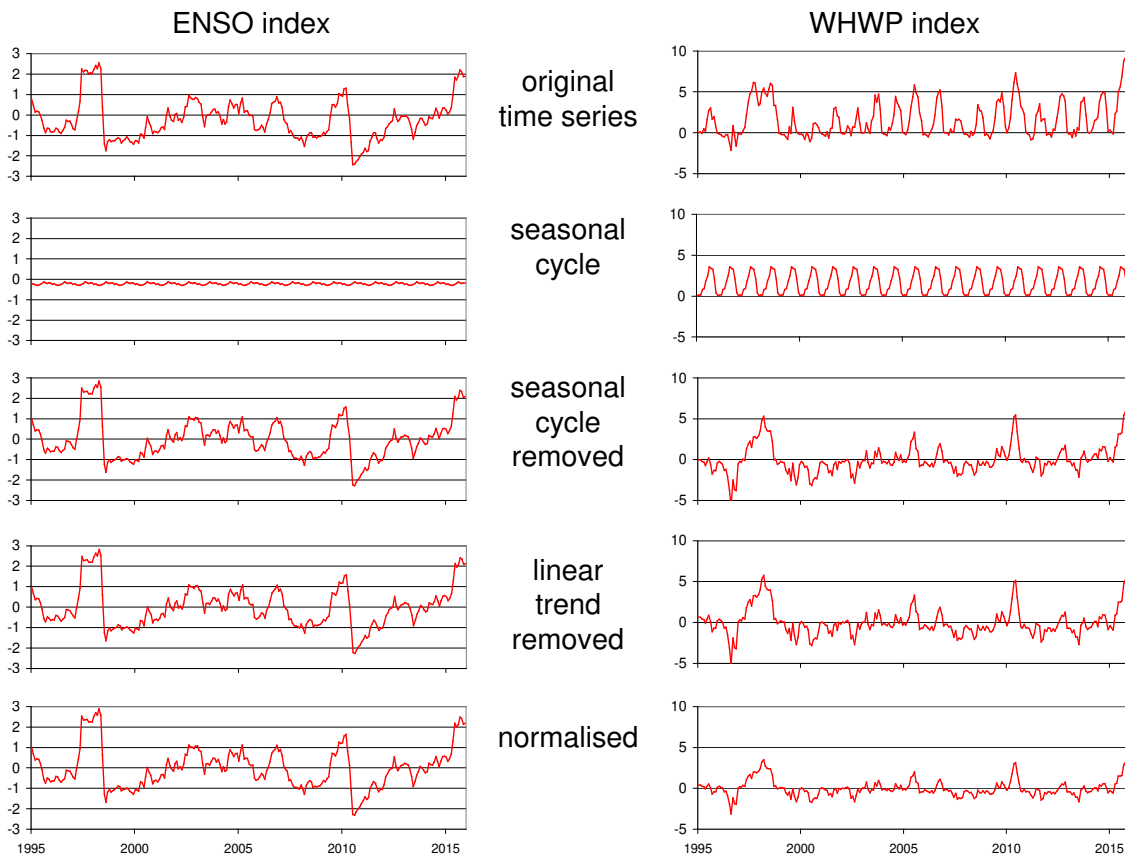
**Fig. A7: Illustration of the preparations for the indices before they are used in the fit to the global data sets: First, the mean seasonal cycles and linear trends are subtracted. Then the differences are normalised by their standard deviations.**
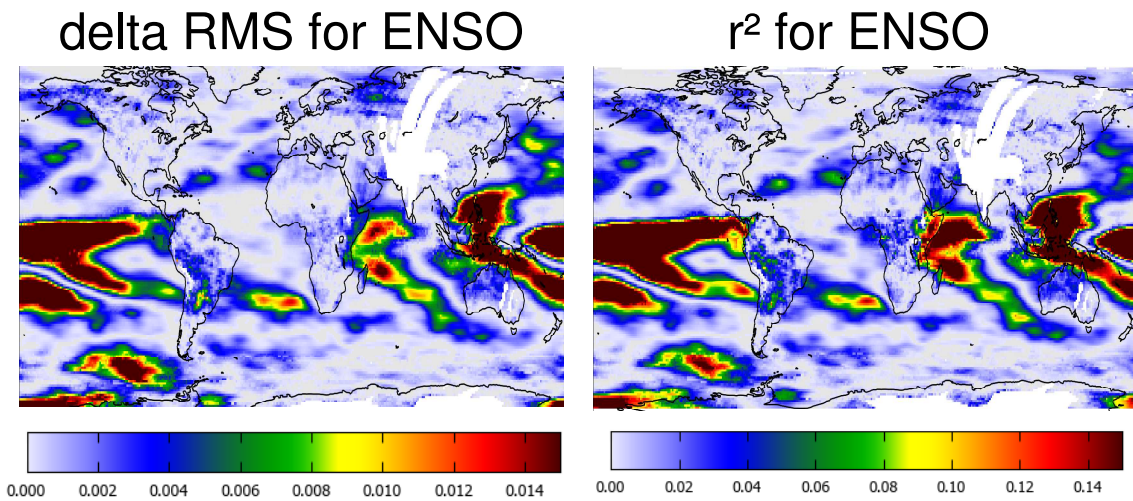
**Fig. A8: Delta RMS (left) and r² values (right) for the fit of the ENSO index to the TCWV derived from satellite observations.**

**MJO Indices**
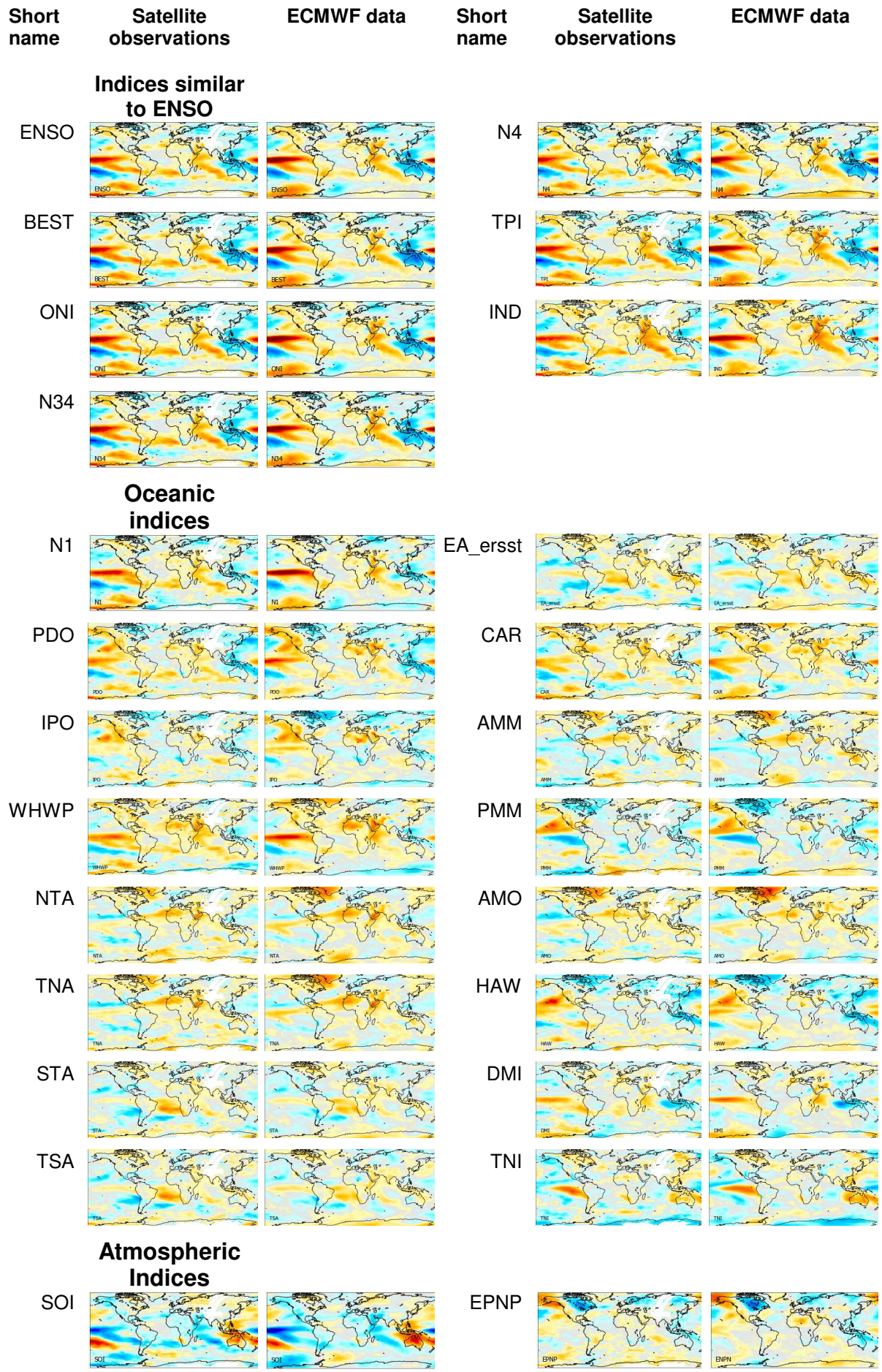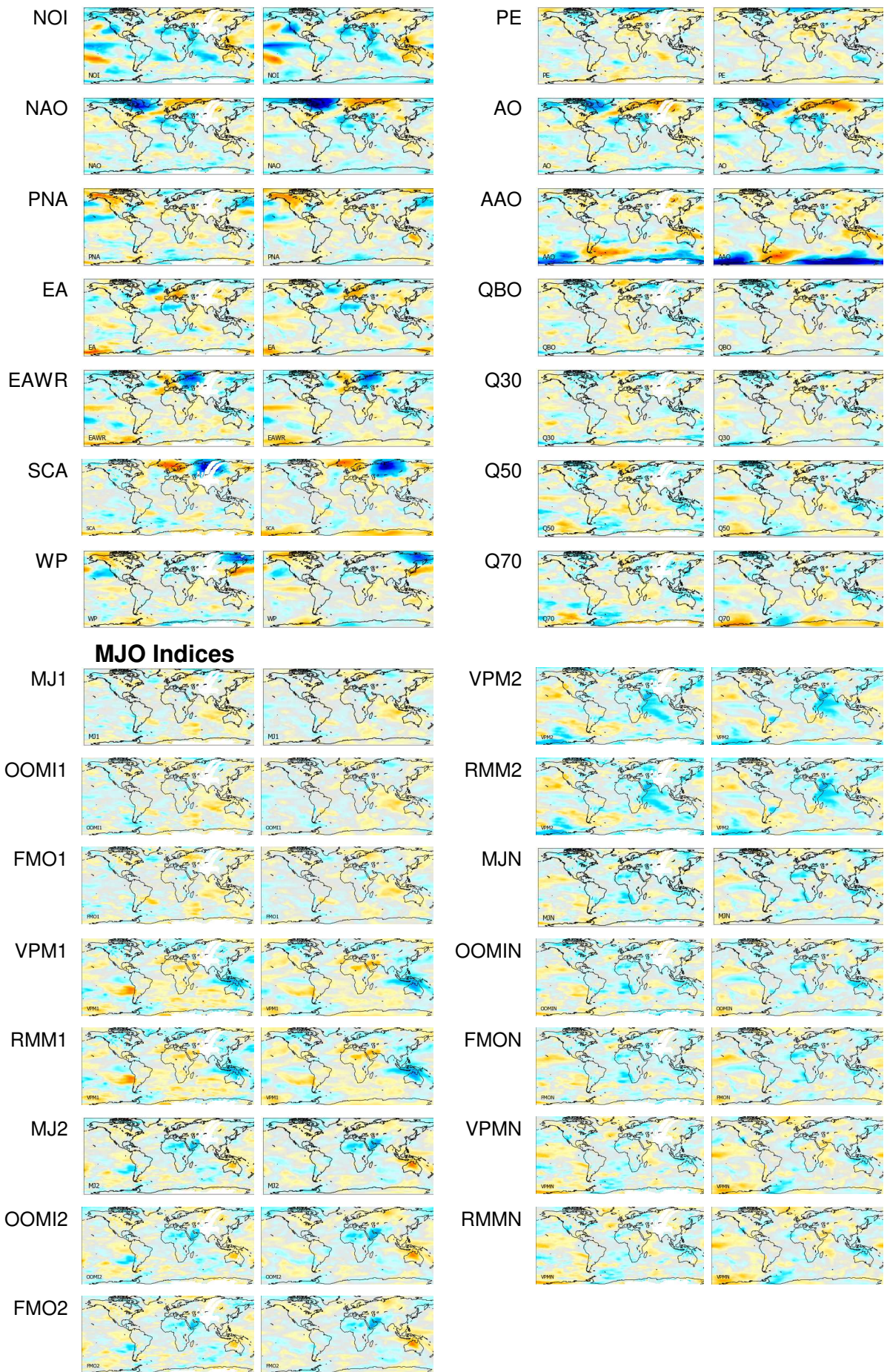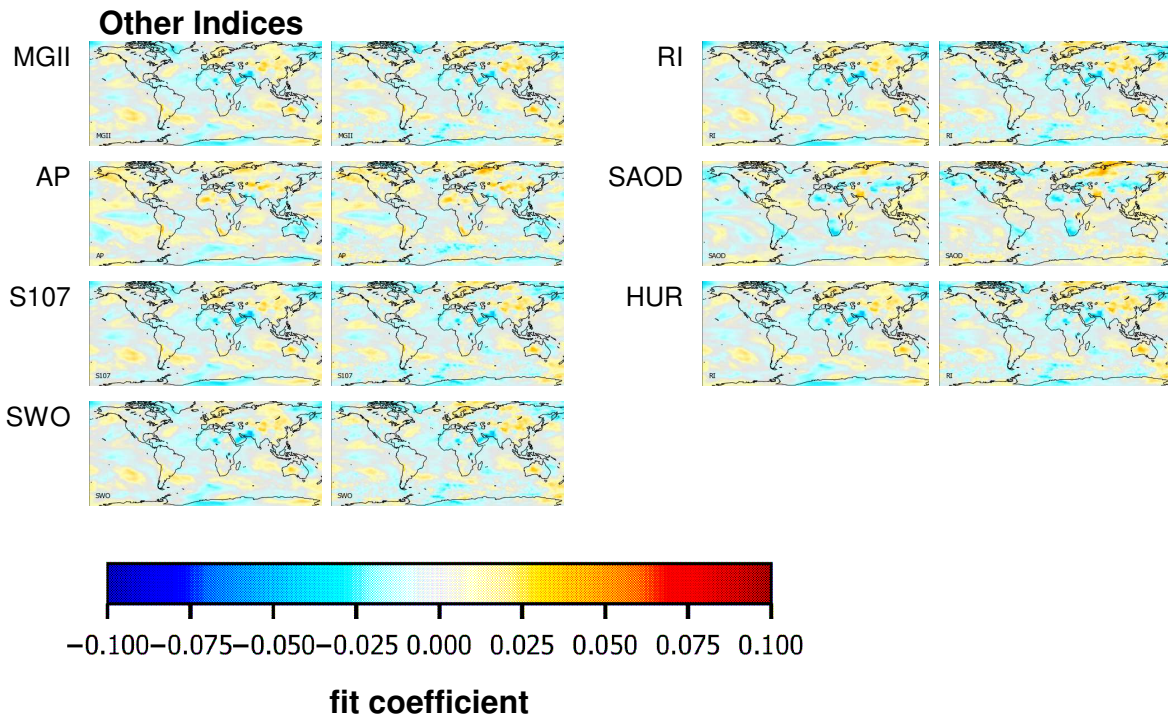
**Fig. A9: Fit coefficients for all indices used in this study. Shown are the results for the TCWV data set from satellite observations (left) and model results (for all sky conditions) (right).**
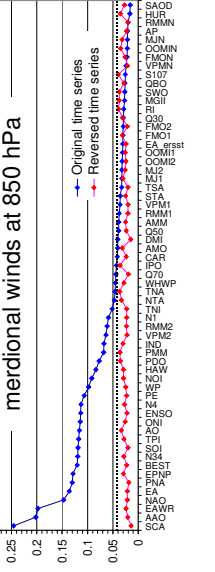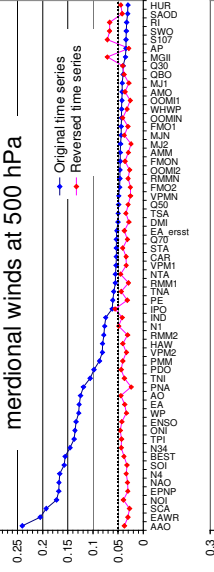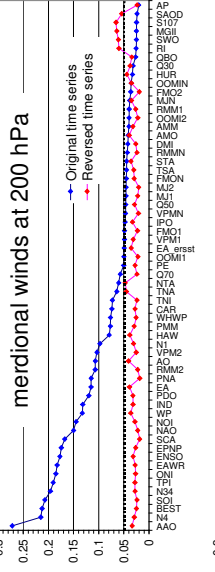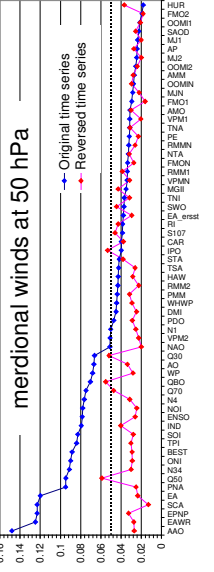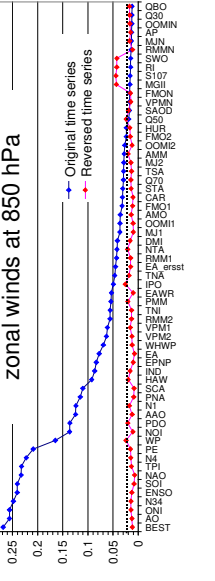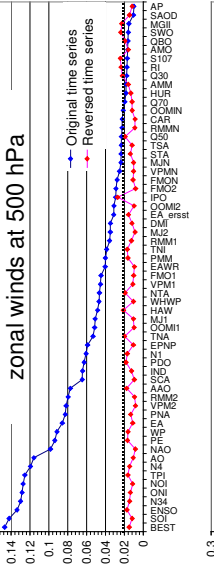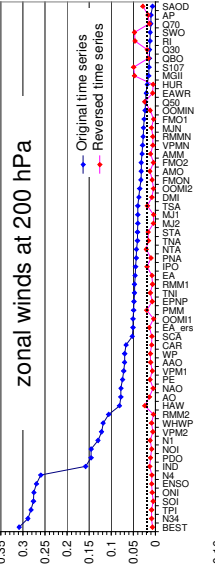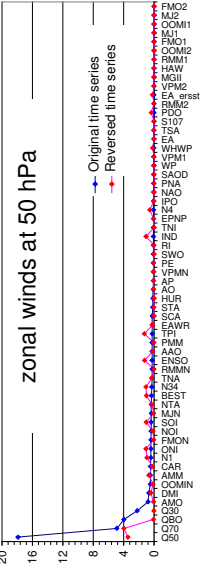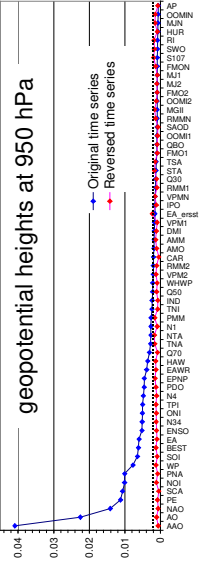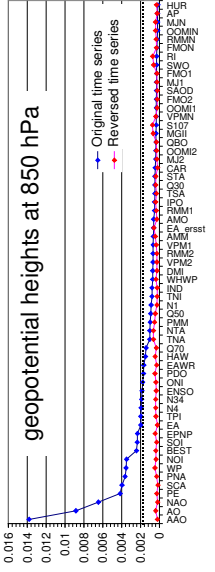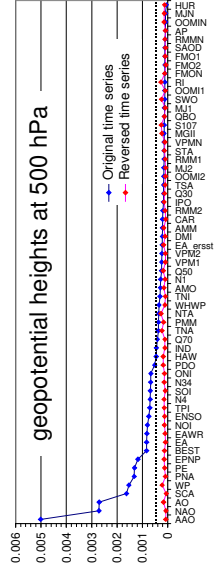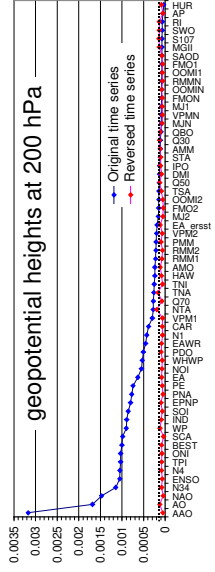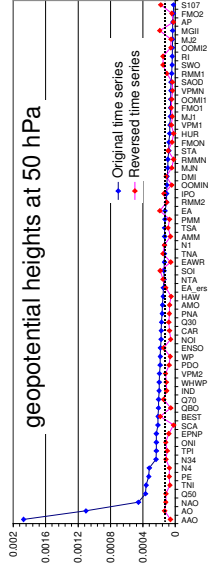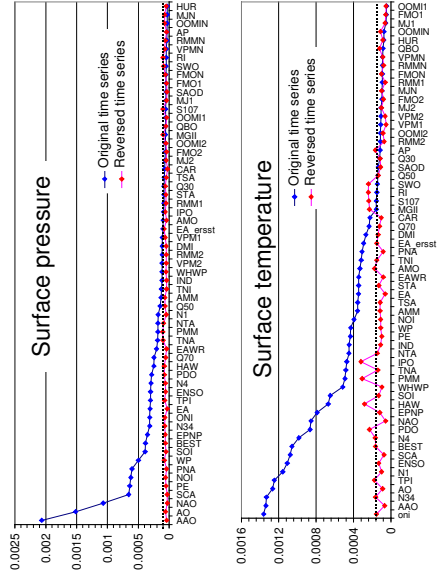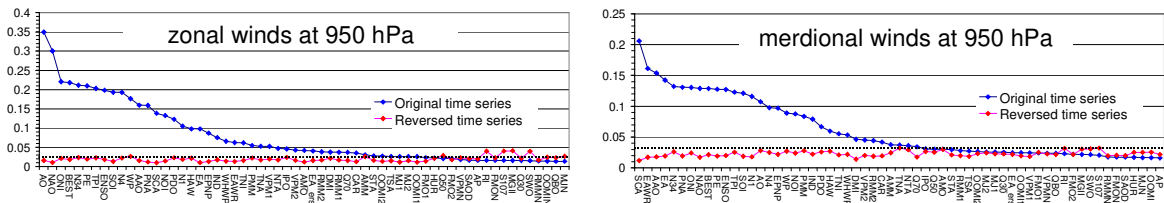
**Fig. A10: 99th percentiles of the delta RMS values (p99) found for the different indices in different global data sets. Blue markers: p99 for the original indices; red markers: p99 for the temporally reversed indices; black lines: significance thresholds. The indices are sorted from highest to lowest p99 values for the original indices.**
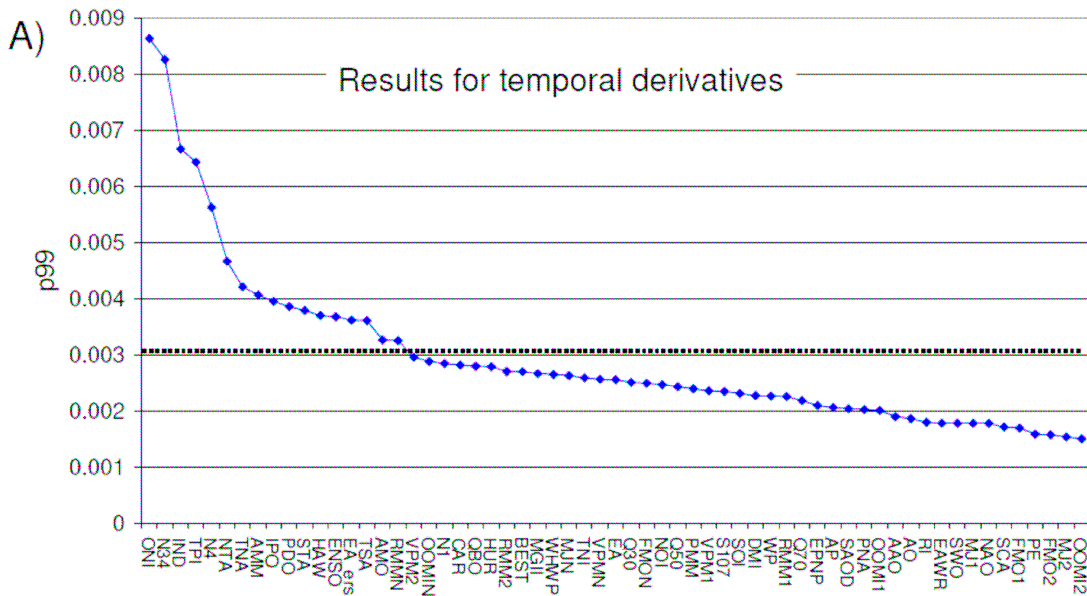
1055

1060

**Fig. A11. The 99th percentiles (p99) of the delta RMS of the derivatives of all indices. The black lines represent the significance threshold. The indices are sorted from highest to lowest p99 values.**

1065

1070

1075

1080

1085

1090
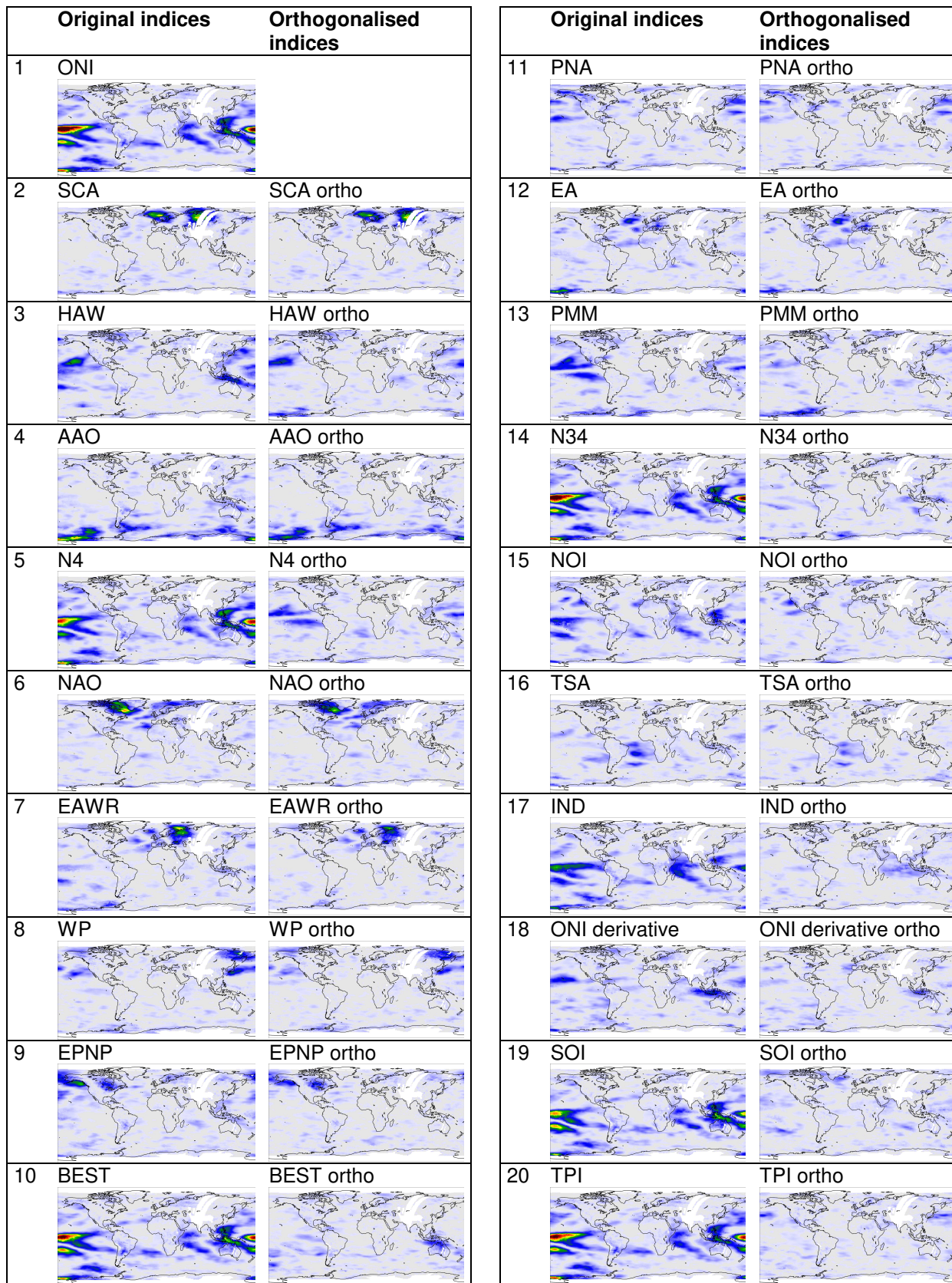
**Fig. A12: Delta RMS maps for the significant orthogonalised indices together with the delta RMS maps for the original indices. The numbers at the left sides indicate the order (descending) of the p99 values (see also Fig. 9).**

1095

**Table A1 Significant indices for all data sets (indices with p99 values below threshold but shift ratios <0.8 are indicated in brackets).**

| Data set | Number of significant indices | Significant indices (from highest to lowest p99 values) |
|---|---|---|
| TCWV sat | 42 (2) | ONI, N34, TPI, ENSO, BEST, N4, N1, SOI, IND, HAW, PDO, PMM, AAO, SCA, WHWP, NOI, NAO, TNI, WP, EAWR, DMI, EPNP, CAR, PNA, VPM1, AO, VPM2, TSA, STA, TNA, EA, EA_ersst, AMO, RMM2, NTA, AMM, RMM1, IPO, Q50, Q70 (PE, MJ2) |
| TCWV ERA | 44 (1) | ONI, N34, ENSO, TPI, BEST, N1, N4, SOI, IND, AAO, WHWP, NOI, PDO, SCA, NAO, HAW, PMM, EPNP, TNI, DMI, VPM1, AO, WP, EAWR, CAR, TNA, NTA, PNA, RMM1, VPM2, AMO, IPO, STA, RMM2, TSA, EA, AMM, EA_ersst, MJ2, Q70, FMO2, OOMI2, VPMN, Q50 (PE) |
| TCWV ERA clear | 42 (3) | ONI, N34, ENSO, TPI, N1, BEST, N4, SOI, IND, AAO, WHWP, PDO, NOI, SCA, HAW, NAO, TNI, DMI, PMM, EPNP, WP, VPM1, EAWR, CAR, AO, PNA, TNA, VPM2, NTA, IPO, AMO, TSA, EA_ersst, STA, RMM2, RMM1, AMM, EA (PE, FMO2, OOMI2) |
| Tsurf | 37 (1) | ONI, AAO, N34, AO, TPI, N1, ENSO, SCA, BEST, N4, PDO, NAO, EPNP, HAW, SOI, WHWP, PMM, TNA, IPO, NTA, IND, PE, WP, NOI, AMM, TSA, EA, STA, EAWR, AMO, TNI, PNA, EA_ersst, DMI, Q70, CAR (RMM2) |
| Spred | 35 (1) | AAO, AO, NAO, SCA, PE, NOI, PNA, WP, SOI, BEST, EPNP, N34, ONI, EA, TPI, ENSO, N4, PDO, HAW, Q70, EAWR, TNA, PMM, NTA, N1, Q50, AMM, TNI, IND, WHWP, VPM2, RMM2, DMI, VPM1 (RMM1) |
| Geopot 50 hPa | 17 (5) | AAO, AO, NAO, Q50, TNI, PE, N4, N34, TPI, ONI, EPNP (VPM2, PNA, EA, RMM2, RMMN) |
| Geopot 200 hPa | 40 (0) | AAO, AO, NAO, N34, ENSO, N4, TPI, ONI, BEST, SCA, WP, IND, SOI, EPNP, PNA, PE, EA, NOI, WHWP, PDO, EAWR, N1, CAR, VPM1, NTA, Q70, TNA, TNI, HAW, AMO, RMM1, RMM2, PMM, VPM2, EA_ersst, MJ2, FMO2, OOMI2, TSA |
| Geopot 500 hPa | 32 (1) | AAO, NAO, AO, SCA, WP, PNA, PE, EPNP, BEST, EA, EAWR, NOI, ENSO, TPI, N4, SOI, N34, ONI, PDO, HAW, IND, Q70, TNA, PMM, NTA, WHWP, TNI, AMO, N1, Q50 (RMM2) |
| Geopot 850 hPa | 33 (1) | AAO, AO, NAO, PE, SCA, PNA, WP, NOI, BEST, SOI, EPNP, EA, TPI, N4, N34, ENSO, ONI, PDO, EAWR, HAW, Q70, TNA, NTA, PMM, Q50, N1, TNI, IND, WHWP, DMI, VPM2 (RMM1) |
| Geopot 950 hPa | 30 (1) | AAO, AO, NAO, PE, SCA, NOI, PNA, WP, SOI, BEST, EA, ENSO, N34, ONI, TPI, N4, PDO, EPNP, EAWR, HAW, Q70, TNA, NTA, N1, PMM, TNI, IND, Q50 (RMM2) |
| Zonal winds 200 hPa | 51 (0) | BEST, N34, TPI, SOI, ONI, ENSO, N4, IND, PDO, NOI, N1, VPM2, WHWP, RMM2, HAW, AO, NAO, PE, VPM1, AAO, WP, CAR, SCA, EA_ersst, OOMI1, PMM, EPNP, TNI, RMM1, EA, IPO, PNA, NTA, TNA, STA, MJ2, MJ1, TSA, DMI, OOMI2, FMON, AMO, FMO2, AMM, VPMN, RMMN, MJN, FMO1, OOMIN, Q50 |
| Zonal winds 500 hPa | 49 (0) | BEST, SOI, ENSO, N34, ONI, NOI, TPI, N4, AO, NAO, PE, WP, EA, PNA, VPM2, RMM2, AAO, SCA, IND, PDO, N1, EPNP, TNA, OOMI1, MJ1, HAW, WHWP, NTA, VPM1, FMO1, EAWR, PMM, TNI, RMM1, MJ2, DMI, EA_ersst, OOMI2, IPO, FMO2, FMON, VPMN, MJN, STA, TSA, Q50, RMMN, CAR, OOMIN |
| Zonal winds 850 hPa | 46 (1) | BEST, AO, ONI, N34, ENSO, SOI, NAO, TPI, N4, PE, WP, NOI, PDO, AAO, N1, PNA, SCA, HAW, IND, EPNP, EA, WHWP, VPM2, VPM1, RMM2, TNI, PMM, EAWR, IPO, TNA, EA_ersst, RMM1, NTA, DMI, MJ1, OOMI1, AMO, FMO1, CAR, STA, Q70, TSA, MJ2, AMM, OOMI2 (FMO2) |
| Zonal winds 950 hPa | 42 (4) | AO, NAO, ONI, BEST, N34, PE, TPI, ENSO, SOI, N4, WP, AAO, PNA, SCA, NOI, PDO, N1, HAW, EA, EPNP, IND, WHWP, EAWR, TNI, PMM, TNA, VPM1, NTA, IPO, VPM2, AMO, EA_ersst, RMM2, DMI, RMM1, Q70, CAR, AMM (OOMI2, MJ1, MJ2, OOMI1) |
| Meridional winds 50 hPa | 24 (3) | AAO, EAWR, EPNP, SCA, EA, PNA, Q50, N34, ONI, BEST, TPI, SOI, IND, ENSO, NOI, N4, Q70, QBO, WP, AO (VPM2, RMM2, PE) |
| Meridional winds 200 hPa | 32 (1) | AAO, N4, BEST, SOI, N34, TPI, ONI, EAWR, ENSO, EPNP, SCA, NAO, NOI, WP, IND, PDO, EA, PNA, RMM2, AO, VPM2, N1, HAW, PMM, WHWP, CAR, TNI, TNA, NTA, Q70 (FMO1) |
| Meridional winds 500 hPa | 34 (0) | AAO, EAWR, SCA, NOI, EPNP, NAO, N4, SOI, BEST, N34, TPI, ONI, ENSO, WP, EA, AO, PNA, TNI, PDO, PMM, VPM2, HAW, RMM2, N1, IND, IPO, PE, TNA, RMM1, NTA, VPM1, CAR, STA |

| Meridional winds 850 hPa | 33 (0) | SCA, AAO, EAWR, NAO, EA, PNA, EPNP, BEST, N34, SOI, TPI, AO, ONI, ENSO, N4, PE, WP, NOI, HAW, PDO, PMM, IND, VPM2, RMM2, N1, TNI, NTA, TNA, WHWP, Q70, IPO, CAR |
|---|---|---|
| Meridional winds 950 hPa | 32 (0) | SCA, EAWR, AAO, EA, N34, PNA, ONI, NAO, BEST, PE, ENSO, TPI, SOI, N1, AO, N4, EPNP, WP, NOI, PMM, IND, PDO, HAW, TNI, WHWP, DMI, VPM2, RMM2, CAR, AMM, TNA |

1105